CrossMark

Multi-scale Structural Modeling of Soft Tissues Mechanics and Mechanobiology

Yoram Lanir[1] ⓘD

Abstract Soft tissues account for a major fraction of the body volume and mass. They are present in all non-skeletal organs, being responsible for protecting the body, maintaining internal homeostasis, and allowing for mobility. Their function in different organs is highly diverse, as are their properties which are optimally suited for their specific tasks. From a mechanical perspective, specificity of structure and properties is acquired via evolutionary adaptation of the tissue composition and multi-scale structure. In modeling tissue mechanics and mechano-biology, it is thus natural to seek the structural determinants of tissues and their evolution (the "structural approach"). Earlier models were exclusively phenomenological, based either on the general principles of non-linear continuum mechanics or alternatively, on empirical mathematical expressions that fit specific response patterns. In the late 1970's, structural models were introduced to tissue mechanics (Lanir in J. Biomechanics 12(6): 423–436, 1979; Lanir in J. Biomechanics 16(1): 1–12, 1983). Ever since, a gradually increasing number of structural models have been developed for different types of tissues, and today, it is the method of choice (Cowin and Humphrey in J. Elasticity 61: ix–xii, 2000). The structural approach was recently extended to incorporate a mechanistic formulation of mechano-biological pathways by which tissue structures remodel during growth (Lanir in Biomech Model Mechanobiol, 14(2): 245–266, 2015). Here, the characteristic features of soft tissue structures and their constitutive modeling are reviewed. The presentation starts with a brief survey of the multi-scale and multi-phasic soft tissues structure. The global mechanical characteristics of soft tissues and of their constituents are then briefly reviewed. These two aspects form the basis for structural constitutive formulation via the multi-scale structure-function link. Based on established criteria for model validity, predictions of the formulated theory are contrasted against measured response characteristics. Using this structure-function relationship, the evolutionary pathway by which tissue structure and mechanics remodel during growth to adapt to their physiological function, is laid down. The review concludes with an account of the state of the art, the big picture, and future research challenges in tissue mechanobiological modeling.

✉ Y. Lanir
yoramlanir@yahoo.com

[1] Faculty of Biomedical Engineering, Technion – IIT, Haifa 32000, Israel

Abbreviations
CSK   Cytoskeleton
CVS   Cardiovascular system
ECM   Extra-cellular matrix
G&R   Growth and remodeling
GAG   Glycosaminoglycans
LM   Light microscopy
LVE   Linear viscoelasticity
LV   Left ventricle
OA   Opening angle
PC   Preconditioning
PG   Proteoglycans
QLV   Quasilinear viscoelasticity
REV   Representative elementary volume
RPC   Recruitment preconditioning
RS   Residual stress
RVE   Recruitment viscoelasticity
SEM   Scanning electron microscopy
VE   Viscoelasticity
1D, 2D, 3D One-, two-, and three-dimensional

1 Introduction

The foundations of modern soft tissues mechanics were established by Y.C. Fung, starting in the late 1960s [1]. Over the years, Fung introduced the concepts of pseudo-elasticity, exponential stress-strain models, quasilinear viscoelasticity, preconditioning and residual stress, which are cornerstones of the field till today. Fung's models are based on non-linear continuum mechanics, and are phenomenological in nature. As such, their material parameters bear no physical meaning. In view of the large inter-specimen biological variability, where each tissue sample can have its own mechanical properties, lack of physical meaning implies that there is no common denominator which can serve to unify and project between different specimen and tissues. In the late 1970s structure-based multi-scale approach was introduced to tissue modeling wherein parameters have clear physical or structural meaning and structure serves as the common determinant of properties.

This review is dedicated to structural modeling of soft tissues mechanics and mechanobiology. Structural models are important not only in their potential to unify apparently unrelated observations into a coherent framework but also in facilitating insight into the underlying processes and their interactions, thereby providing the groundwork for hypotheses testing of the role and significance of the system processes. Space limitations did not allow for including a review of various semi-structural and structure-motivated model which are partially phenomenological. Two recent reports provide historical background of the structural approach to tissue characterization. One is a personal account of the conception of the structural approach [2]. The other [3] is an insightful review of the history of structural constitutive models.

1.1 Soft Tissue Multi-scale Structure

Soft tissues exhibit a variety of structures, compositions and properties which render them highly suitable for their physiological functions. The structure of each tissue is a multi-scale hierarchy of elements from the molecules through cells, micro-fibrils and fibers, to the tissue level. Mechanically, the predominant elements are the fibers, the fluid-like matrix, and the excitable muscle cells in active tissues. The protein fibers are primarily non-excitable collagen and elastin fibers, and fibronectins and laminins micro-fibers which are mechanically less significant. Collagen is the structural building block of tendons, skin, blood vessels, cornea, sclera, cartilage, intervertebral discs, bones, fascia and uterus cervix. Elastin fibers are found in vertebrate skin, walls of arteries and veins, the lung parenchyma, and in the ligamentum nuchae of horses and cows. Each fiber is itself a multi-scale structure. Collagen is made of distinct fibrils, each of which is a multi-scale system ranging from the fibril down to the sub-fibrils, the highly structured micro-fibrils, and ending in the triple-helical tropo-collagen molecule composed of three amino acid alpha chains [4]. Elastin fibers consist of two proteins, an amorphous insoluble elastin and an elastic micro-fibril composed primarily of the glycoprotein fibrillin [5]. The structure of the fiber network is highly variable. In some tissues the fibers are organized in parallel orientation (collagen in tendons and ligaments, elastin in ligament nuchae), while in others the networks are planar (the skin, heart valve leaflets, body membranes), or are in association with the tissue cells in a more complex there-dimensional manner (e.g., elastin and collagen in blood vessels, collagen and myocytes in the heart [6, 7]).

The matrix of soft tissues is comprised of a water solvent containing solutes of ions, protein molecules and very large proteoglycans (PGs) which are encaged within the tissue fiber networks. PGs are complex macromolecules which are made of a protein core with covalently bound negatively charged glycosaminoglycan (GAG) chains. The fixed charges of the GAG chains endow the matrix with osmotic pressure which attracts water and swells the tissue up to equilibrium where the matrix pressure is mechanically counter-balanced by tension in the tissue fibers [8]. Hence soft tissues are well hydrated thereby benefiting from a plasticizing effect [9].

The cells in soft tissues are of different types and functions. They can have distinct disposition within the tissue system. Whereas some smooth muscle cells (depending on the tissue type), and other non-contractile cells are often found dispersed within the fiber network, arterial smooth muscle cells (SMCs) are encaged within the media inter-lamellar elastin network with approximately circumferential disposition. In the bladder the SMCs are organized in three distinct, closely packed sub-layers within the detrusor layer of the wall. In the heart wall, the myocytes are circumferentially organized parallel to each other in an orientation which changes gradually between the inner endocardium to the outer epicardium surfaces. In skeletal muscle, the cells are long, and span the entire length of the muscle.

Each cell is by itself a multi-scale system, ranging from the molecular level, via the cytoskeleton (CSK), to the whole-cell level. In non-muscle cells, the dynamic CSK consists of actin and microtubule filaments and of dispersed acto-myosin motor units, which enable active contraction of the cells. Muscle cells contain highly organized contracting sarcomere units made of inter-digitating actin and myosin filaments, and of non-contracting titin protein filaments which protect the sarcomeres from over-stretch.

1.2 Soft Tissues Mechanical Properties

Soft tissues undergo finite reversible deformations, at times stretching by 100 % or more (e.g., skin, mesentery membrane). Their stress-strain relationship is convexly non-linear,

where the stiffness increases with tensile strain. Their response is in general anisotropic as well as time-dependent, subject to reversible (with time) viscoelasticity, and to irreversible preconditioning adaptation [10–13]. Viscoelasticity is manifested as creep under constant stress, stress relaxation under constant strain and onset of a hysteresis loop between loading and unloading responses. Tissue preconditioning is seen under repeated cycles of stretch, where the stress decays asymptotically with cycle number until reaching a stable response. Under *in vitro* conditions the effects of preconditioning are only partially reversible after a long rest period. Importantly, the tissue response depends on its preconditioning protocol, implying that any change in the testing protocol may require a new round of preconditioning [14, 15].

Residual Stress and Strain (*RS*): In their unloaded state, tissues are not stress-free but are subjected to internal residual stress and to its associated residual strain. In arteries, it was found [16, 17] that when an artery ring is cut longitudinally, it springs open with an opening angle (OA) whose magnitude was taken to be a measure of the RS level. A similar phenomenon was found in left ventricle (LV) myocardial rings [18, 19].

Importantly, RS must be incorporated in tissue stress analysis since the true fibers' strain (and the resulting true tissue stress) is the one referenced to the stress-free state at which all fibers are un-stretched and stress-free [20, 21]. The true strain and associate true stress determine the actual mechanical environment of the tissue cells, to which they can respond by remodeling their extra-cellular matrix (ECM). In addition, Fung and others showed that RS significantly affects the tissue's stress and strain distributions, and carries substantial functional benefits by reducing stress concentration near the internal surface of arteries and LV and by increasing the compliance of the latter during the diastolic feeling phase, thereby improving its blood pumping performance [16, 19, 22, 23].

1.3 Mechanics of Tissues' Constituents

Tissue fibers are thin and long. When contracted, they buckle under very low load and assume an undulated (wavy) disposition. This is often seen in collagen fibers in unloaded tissues. The level of fiber undulation is non-uniformly distributed amongst the fibers. Upon stretch, the fibers become gradually straight and load-bearing [24–26], thereby increasing the tissue stiffness. The straight collagen fiber is stiff, with an axial modulus ranging (depending on the species and tissue) between 100 MPa and 1200 MPa [27]. It can be reversibly stretched up to 5–8 %. Collagen fibers are viscoelastic and undergo preconditioning adaptation under repeated stretch cycles. Elastin is close to being purely elastic, and is highly extensible being able to reversibly stretch by 100 % and more. Its stress-strain response is linear up to approximately 60 % stretch and then curves up to a convex response. In the linear range, the elastin stiffness is approximately (depending on the tissue) two orders of magnitude lower than that of the collagen, i.e., approximately 1 MPa, as measured in bovine ligamentum nuchae [28] and as estimated for elastin in the skin [14].

Tissue cells are of two classes, muscle and non-muscle cells. In non-muscle cells such as fibroblasts, the CSK is highly dynamic, and constantly subjected to actin filaments polarization/depolarization, and to spontaneous activity of its acto-myosin motor units. The cells need a homeostatic mechanical environment in order survive and proliferate [29]. They achieve this by adapting their extra-cellular fiber matrix (ECM) and by exerting traction on the ECM fibers, at a level which is cell- and tissue-specific [30, 31]. Traction is produced either passively by the intra-cellular actin cytoskeleton [32], or actively by the motor units [33]. In muscle cells, all three types (skeletal, myocytes and smooth muscle) share the actin-myosin contractile unit. Yet, there are important mechanical differences between them. In

response to a single short stimulus (twitch), a skeletal muscle contracts and subsequently relaxes rapidly (it has a short refractory period). Successive twitches add up to produce stronger response (by wave summation) which increases with frequency up to a tetanized state at which the force can be maintained for a long period [34]. Cardiac myocytes on the other hand, cannot tetanize. They contract rapidly but have a longer refractory period during which they cannot be re-excited, a pre-requisite feature for the rhythmic contraction and blood pumping function of the heart. While some SMCs properties are similar to those of skeleton and cardiac muscle [35], they contract slowly. Some contract rhythmically in organs producing peristaltic motion (e.g., ureter and intestine) while others (e.g., in the arterial wall) maintain constant contraction force for very long periods, thereby maintaining a controlled vessel diameter and blood supply as required by the organ. Smooth muscle lining the walls of some hollow organs possess a malleable contractile apparatus—their cytoskeleton and sarcomeres can modify both their structure and number in series to adapt to large length changes. This length adaptation does not change their passive tension nor their active isomeric force [36–40]. An extreme example are smooth muscle cells in the bladder wall, which increase their length by a factor of up to 2.0–2.2 under low urine pressure as the bladder is gradually filled up to 7–10 times its empty volume. When activated, these cells contract and reduce their reference length back to its initial level within seconds as the bladder is emptied.

2 Multi-scale Structural Modeling of Tissue Mechanics

Updated reviews of soft tissues structure-motivated and structural models have recently been published [3, 41–53]. Here, the focus will be on fully structural modeling.

The determinants of soft tissue response are its constituents' structure and mechanics, the manner by which structure changes with deformation, the kinematic response of each constituent to the deformation, and the way by which the contributions of all constituents are integrated to yield the global tissue response.

Experimental observations revealed that in the stretched tendon [26, 54] and skin [24], there is a gradual straightening (recruitment) with stretch of initially undulated collagen fibers, and this is accompanied by an increase in the tissue stiffness. A similar gradual straightening was observed in bi-axially stretched mesentery [25]. In addition to their undulation, observations have revealed that in flat tissues the fibers' orientation is dispersed [25], and that in response to tissue deformation the fibers rotate towards the direction of highest stretch [24, 55]. The quantitative correlates of these observations which are needed for structural constitutive formulation, are based on the following assumptions [56, 57] which are derived from direct observations and measured data.

2.1 Basic Assumptions

Assumption B1 Soft tissues consist of fibers and cells embedded in a matrix of fluid ground substance.

Assumption B2 There are no voids in the tissue space.

Assumption B3 All constituents are incompressible, and so is the tissue as a whole under short loading protocols during which there is insufficient time for fluid to filtrate in or out of the tissue space.

Fig. 1 Mapping scheme
between the stress-free, unloaded
and loaded fiber network and
tissue. The $\boldsymbol{B}$'s designate the
tissue and network configurations
$\boldsymbol{F}$'s are the deformation
gradients, and $\boldsymbol{\Sigma}$'s are the
Cauchy stresses. Superscript
SF—stress free, *UL*—Unloaded
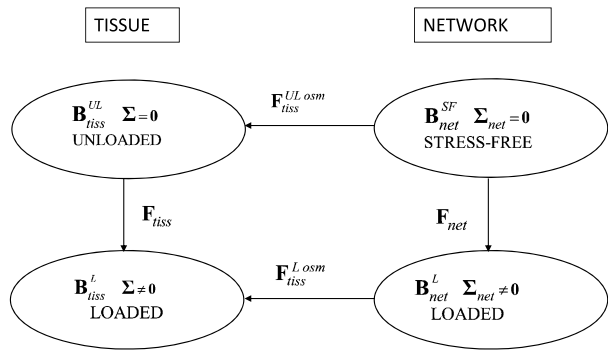
Assumption B4 Tension in the fibers and muscle cells are functions of their axial deformation. Being thin and long, the fibers buckle under contraction thereby losing their stiffness.

Assumption B5 The strain in each constituent is equal to the global tissue strain (affine deformation) [52, 58].

Assumption B6 The global tissue response to loading equals the sum contributions of its solid constituents and of the matrix hydrostatic pressure (rule of mixtures).

2.2 Tissue Kinematics

The formulation considers a tissue representative elementary volume (REV) whose dimensions are small enough compared to those of the whole tissue/organ so that its strain can be regarded as locally homogeneous, yet large enough (compared with the tissue cells and fibers) to be statistically representative of the local tissue structure, kinematics and properties. Since the tissue is initially swollen by the matrix pressure from a stress-free to an unloaded state, two reference configurations and two loaded ones are considered (Fig. 1). The mapping between each two REV configurations is prescribed by the associated deformation gradient $\mathbf{F} \equiv \partial\mathbf{x}/\partial\mathbf{X}$ where $\mathbf{X}$ and $\mathbf{x}$ are respectively the REV coordinates prior to and following the deformation. Associated with each deformation gradient $\mathbf{F}$ are the right Cauchy-Green deformation tensor $\mathbf{C} = \mathbf{F}^T\mathbf{F}$ and the Lagrangian Green strain $\mathbf{E} = (\mathbf{C}-\mathbf{I})/2$. In view of the scheme in Fig. 1 and to simplify the notation, unless otherwise specified, these deformation metrics relate to the fiber network.

2.3 Mechanics of Single Fibers

In most soft tissues the collagen fibers are buckled and undulated in the stress-free state. A single fiber is characterized by its straightening stretch λ_s under which it becomes straight and tension bearing. When stretched in the loaded state by stretch ratio λ, its true stretch λ_f is

$$\lambda_f = \begin{cases} \lambda/\lambda_s & \forall \lambda > \lambda_s \text{ stretched,} \\ 1 & \forall \lambda \leq \lambda_s \text{ buckled, unstretched.} \end{cases} \tag{2.1}$$

The strains corresponding to each of the stretches $\lambda_s, \lambda, \lambda_f$ are related to them by $e = (\lambda^2 - 1)/2$. Substitution into Eq. (2.1) yields the true fiber strain in terms of its global (e) and

straightening strains (e_s)

$$e_f = \begin{cases} (e - e_s)/(1 + 2e_s) & \forall e > e_s \text{ stretched,} \\ 0 & \forall e \leq e_s \text{ buckled, unstretched.} \end{cases} \tag{2.2}$$

If the fiber is hyper-elastic then its strain energy function under adiabatic or isothermal conditions depends solely on its true strain, i.e., $w_f = w_f(e_f)$. Its second Piola-Kirchoff stress is $s_f(e_f) = \partial w_f/\partial e_f$. In view of its incompressibility (Assumption B3) the fiber's first Piola-Kirchhoff and Cauchy's stress are related to its second Piola-Kirchhoff stress by $t_f = \lambda_f \cdot s_f$ and $\sigma_f = \lambda_f^2 \cdot s_f$, respectively.

2.4 Mechanics of Uniaxial Fiber Bundles

A fiber bundle consists of the network fibers sharing a similar orientation in the initial reference configuration. By affine deformation (Assumption B5), the bundle and its fibers rotate and stretch during deformation in mutually similar magnitudes and thus, share similar deformed orientation. Hence, for all bundle fibers $\lambda = \Lambda_{bun}$, $e = E_{bun}$. In addition, a bundle (and its fibers) having an initial orientation $\mathbf{N}$ (a unit vector with a solid angle Ω with respect to a given Cartesian coordinate system) will assume an orientation $\hat{\mathbf{n}}$ (a unit vector) in the deformed configuration, where

$$\hat{\mathbf{n}} = \mathbf{n}/|\mathbf{n}|, \quad \mathbf{n} = \mathbf{F} \cdot \mathbf{N}. \tag{2.3}$$

Based again on affine deformation, the bundle and its fibers' stretch and strain in the loaded state are:

$$\Lambda_{bun}(\mathbf{N}) = [\mathbf{N} \cdot \mathbf{CN}]^{1/2}, \qquad E_{bun} = \left((\Lambda_{bun})^2 - 1\right)/2. \tag{2.4}$$

The straightening strains are non-uniformly distributed over the bundle fibers by a density distribution function $D(q, \mathbf{N})$ which is defined as follows: in the bundle of stress-free reference orientation $\mathbf{N}$, the fraction of fiber volume becoming straight between strain levels $e = q$ and $e = q + dq$ is equal to $D(q, \mathbf{N}) \cdot dq$. The term $\mathbf{N}$ in $D(q, \mathbf{N})$ denotes that the recruitment distribution may be orientation-dependent. Normalization requires that $\int_0^{+\infty} D(q, \mathbf{N}) \cdot dq = 1$ for every $\mathbf{N}$.

Since $\lambda = \Lambda_{bun}$, and Λ_{bun} is related to the global strain by affine deformation (Eq. (2.4)) then so is also the fiber global stretch λ. Yet, the fiber true deformation (Eq. (2.1)) is not affine since it is related to the global deformation by the dispersed fiber straightening stretch λ_s when stretched, and is buckled and collapsed when contracted.

In the hyper-elastic case, the bundle strain energy per unit stress-free tissue volume is the sum of strain energies of all its straight and stretched fibers:

$$W_{bun}(E_{bun}, \mathbf{N}) = \phi_f^0 \int_0^{E_{bun}} w_f(e_f) \cdot D(q, \mathbf{N}) \cdot dq \quad \forall \mathbf{N}, \tag{2.5}$$

where ϕ_f^0 is the total fibers volume fraction in the tissue which converts the fibers' strain energy per fibers volume to its level per tissue volume. The bundle second Piola-Kirchhoff stress is derived from its strain energy by chain differentiation:

$$S_{bun}(E_{bun}, \mathbf{N}) = \frac{dW_{bun}}{dE_{bun}}(E_{bun}, \mathbf{N}) = \phi_f^0 \int_0^{E_{bun}} D(q, \mathbf{N}) \cdot \left(\frac{dw_f}{de_f} \cdot \frac{de_f}{dE_{bun}}\right) \cdot dq, \tag{2.6}$$

which in view of Eq. (2.2) and $e = E_{bun}$ yields:

$$S_{bun}(E_{bun}, \mathbf{N}) = \phi_f^0 \cdot \int_0^{E_{bun}} \frac{D(q, \mathbf{N})}{(1+2q)} \cdot s_f(e_f) \cdot dq. \tag{2.7}$$

2.5 Mechanics of Three-Dimensional Networks and Tissues

In 3D tissues made of a single type of fibers, each REV has a 3D network of fibers. Each fiber, in addition to its level of undulation (or alternatively, its straightening strain e_s) in the initial reference configuration (before deformation), is characterized by its orientation $\mathbf{N}$ which features a solid angle Ω. This orientation angle is distributed over the un-deformed fiber population with a characteristic orientation density $\hat{\mathbb{R}}(\Omega)$, such that the volume fraction of the network fibers oriented between the solid angles Ω and $\Omega + d\Omega$ is $\hat{\mathbb{R}}(\mathbf{N}) \cdot d\Omega$. Normalization requires that $\int_\Omega \hat{\mathbb{R}}(\mathbf{N}) \cdot d\Omega = 1$.

In a spherical polar coordinate system (R, Φ, Θ) the fiber's reference orientation $\mathbf{N}$ is expressed as

$$\mathbf{N} = \sin\Phi \cdot \cos\Theta \cdot \mathbf{1}_1 + \sin\Phi \cdot \sin\Theta \cdot \mathbf{1}_2 + \cos\Phi \cdot \mathbf{1}_3, \tag{2.8}$$

where $\mathbf{1}_i$ $(i = 1, 2, 3)$ are unit vectors along the three Cartesian axes. The density normalization condition is expressed as[1,2]

$$\int_0^\pi \int_0^\pi \mathbb{R}(\Phi, \Theta) \cdot d\Phi \cdot d\Theta = 1, \qquad \mathbb{R}(\Phi, \Theta) = \hat{\mathbb{R}}\big(\mathbf{N}(\Phi, \Theta)\big) \cdot \sin\Phi, \tag{2.9}$$

where the $\sin\Phi$ term in $d\Omega = \sin\Phi \cdot d\Theta \cdot d\Phi$ was incorporated into $\mathbb{R}(\Phi, \Theta)$, the modified orientation distribution. The axial strain of the bundle and its fibers is related to the global REV strain $\mathbf{E}$ by affine deformation (Assumption B5), namely

$$E_{bun} = \mathbf{N} \cdot \mathbf{EN} = E_{11} \sin^2\Phi \cdot \cos^2\Theta + E_{22} \sin^2\Phi \cdot \sin^2\Theta + E_{33} \cos^2\Phi$$
$$+ 2E_{12} \sin^2\Phi \cdot \sin\Theta \cdot \cos\Theta + 2E_{13} \sin\Phi \cdot \cos\Phi \cdot \cos\Theta$$
$$+ 2E_{23} \sin\Phi \cdot \cos\Phi \cdot \sin\Theta, \tag{2.10}$$

where E_{ij} $(i, j = 1, 2, 3)$ are the components of the Green-Lagrange strain $\mathbf{E}$ in a Cartesian system.

The total strain energy in the network fibers equals the sum contributions of all the fibers (Assumption B6), or alternatively, all the fiber bundles. Expressed per un-deformed tissue volume, this strain energy is given by:

$$W_{net}(\mathbf{E}) = \phi_f^0 \sum_{\mathbf{N}} W_{bun}(E_{bun}, \mathbf{N}) = \phi_f^0 \int_\Omega \mathbb{R}(\mathbf{N}) \cdot W_{bun}(E_{bun}, \mathbf{N}) \cdot d\Omega. \tag{2.11}$$

The second Piola-Kirchhoff network stress is derived from the strain energy by chain differentiation as follows:

$$\mathbf{S}_{net}(\mathbf{E}) = \frac{\partial W_{net}}{\partial \mathbf{E}} = \int_\Omega \mathbb{R}(\mathbf{N}) \cdot \frac{\partial W_{bun}}{\partial E_{bun}} \cdot \frac{\partial E_{bun}}{\partial \mathbf{E}} \cdot d\Omega. \tag{2.12}$$

---

[1]The integration limits must account for the orientation symmetry since each fiber has two opposite orientations. One possibility for limits is $0 \le \Phi \le \pi$, $0 \le \Theta \le \pi$, another one is $0 \le \Phi \le \pi/2$, $0 \le \Theta \le 2\pi$.

[2]For example, in an isotropic network $\mathbb{R}(\Phi, \Theta) = \sin\Phi/2\pi$.

By using Eqs. (2.6), (2.7) and (2.10) it is seen that

$$\mathbf{S}_{net}(\mathbf{E}) = \phi_f^0 \int_\Omega \mathbb{R}(\mathbf{N}) \cdot \left[\int_0^{E_{bun}(\mathbf{N})} \frac{D(q, \mathbf{N})}{(1+2q)} \cdot s_f(e_f) \cdot dq \right] \cdot \mathbf{N} \otimes \mathbf{N} \cdot d\Omega, \qquad (2.13)$$

where $\mathbf{N} \otimes \mathbf{N}$ is the dyadic product of $\mathbf{N}$ with itself. In polar coordinates Eq. (2.13) is expressed as

$$\mathbf{S}_{net}(\mathbf{E}) = \phi_f^0 \int_0^\pi \int_0^\pi \mathbb{R}(\Phi, \Theta) \cdot \left[\int_0^{E_{bun}(\Phi, \Theta)} \frac{D(q, \mathbf{N}(\Phi, \Theta))}{(1+2q)} \cdot s_f(e_f) \cdot dq \right] \cdot \mathbf{N} \otimes \mathbf{N} \cdot d\Theta \cdot d\Phi. \tag{2.14}$$

The total tissue second Piola-Kirchhoff stress is the sum contributions of its fiber network and matrix pressure P_{mat}. Under short loading protocols the tissue is incompressible (Assumption B3), so that

$$\mathbf{S}_{tiss}(\mathbf{E}) = \mathbf{S}_{net}(\mathbf{E}) - P_{mat}\mathbf{C}^{-1}. \tag{2.15}$$

The network first Piola-Kirchhoff stress expressed in terms of the corresponding fibers stress is given by

$$\mathbf{T}_{net}(\mathbf{E}) = \mathbf{F}\mathbf{S}$$
$$= \phi_f^0 \mathbf{F} \left\{ \int_\Omega \mathbb{R}(\mathbf{N}) \cdot \Lambda_{bun}^{-1}(\mathbf{N}) \cdot \left[\int_0^{E_{bun}(\mathbf{N})} \frac{D(q, \mathbf{N})}{(1+2q)^{1/2}} \cdot t_f(e_f) \cdot dq \right] \cdot \mathbf{N} \otimes \mathbf{N} \cdot d\Omega \right\}, \tag{2.16}$$

where the inner integrand is obtained by inserting $t_f = \lambda_f \cdot s_f$ and $\lambda_f = \Lambda_{bun}/\lambda_s$ (Eq. (2.1)). The global tissue first Piola-Kirchhoff stress is

$$\mathbf{T}_{tiss}(\mathbf{E}) = \mathbf{T}_{net}(\mathbf{E}) - P_{mat}\mathbf{F}^{-T}. \tag{2.17}$$

Finally, the network and tissue Cauchy stresses are, respectively,

$$\Sigma_{net}(\mathbf{E}) = \mathbf{F} \cdot \mathbf{S} \cdot \mathbf{F}^T$$
$$= \phi_f^0 \cdot \mathbf{F} \cdot \left\{ \int_\Omega \mathbb{R}(\mathbf{N}) \cdot \Lambda_{bun}^{-2}(\mathbf{N}) \cdot \left[\int_0^{E_{bun}(\Omega)} D(q, \mathbf{N}) \cdot \sigma_f(e_f) \cdot dq \right] \cdot \mathbf{N}\mathbf{N} \cdot d\Omega \cdot \mathbf{F}^T \right\}, \tag{2.18}$$

$$\Sigma_{tiss}(\mathbf{E}) = \Sigma_{net}(\mathbf{E}) - P_{mat}\mathbf{I}, \tag{2.19}$$

where $\Lambda_{bun} = (1 + 2E_{bun})^{1/2}$ is derived from the REV strain $\mathbf{E}$ by using Eq. (2.10).

2.6 Mechanics of Tissues with Multiple Types of Fibers

In tissues with multiple types of fibers, in general each fiber type i has its own volume fraction $\phi_{f,i}^0$ and mechanical properties $s_f^i(e_f)$. Its network has its own recruitment $D^i(q, \mathbf{N})$ and orientation $\mathbb{R}^i(\mathbf{N})$ distributions. In addition, each network may have its own stress-free reference configuration. The tissue stress-free configuration corresponds to that of the fibers network with the lowest stress-free dimensions (at this configuration no fiber of any type is stretched). For the purpose of constitutive formulation, all networks recruitment and orientation densities should be referenced to that stress-free configuration. The stress derivation

is carried out by summing the contributions of all networks and of the matrix pressure. For example, the second Piola-Kirchhoff stress in the i type network is derived from its fibers' mechanics and densities by:

$$\mathbf{S}_{net}^i(\mathbf{E}) = \phi_{f,i}^0 \int_{\Omega} \mathbb{R}^i(\mathbf{N}) \cdot \left[\int_0^{E_{bun}(\mathbf{N})} \frac{D^i(q, \mathbf{N})}{(1+2q)} \cdot s_f^i(e_f) \cdot dq \right] \cdot \mathbf{N} \otimes \mathbf{N} \cdot d\Omega. \qquad (2.20)$$

The total tissue second Piola-Kirchhoff stress is the sum of all networks stresses and of the matrix pressure,

$$\mathbf{S}_{tiss}(\mathbf{E}) = \sum_i \left[\mathbf{S}_{net}^i(\mathbf{E}) \right] - JP_{mat}\mathbf{C}^{-1}. \qquad (2.21)$$

The first Piola-Kirchhoff and Cauchy stresses are derived in a parallel manner to Eqs. (2.16)–(2.19).

2.7 Validity of Structural Hyper-Elastic Models

Criteria for validity of the constitutive formulation are of two types: general ones which all models must satisfy, and specific ones relating to the model fit to the response of a specific material under a general deformation scheme. Two important general criteria are model convexity (which guarantees physical plausibility) and objectivity (coordinate frame indifference). In contrast to some other hyper-elastic tissue models [59, 60], structural hyper-elastic models were shown [61] to always be convex. The tensor nature of all terms in these models guarantees their objectivity.

Regarding the model fit to response data, experimental tissue characterization should take into consideration the non-linearity of tissue responses and the significant inter-sample biological variability. Non-linear responses can be characterized by a number of models which are indistinguishable in their fit to a given data set (Albert Green, private communication). The challenge is to determine which model is the "true" one. Two measures should be taken to meet this challenge. The first is testing under as many different protocols as possible (e.g., 1D, 2D, and 3D tests under several deformation schemes and strain levels)—only the model which fits well to the response data under all protocols is acceptable. To cope with inter-sample variability, all tests should be carried out on the same sample. Failure to adopt these measures is common in the published literature, thereby casting doubt on the reliability of the models proposed.

The study of Hollander and co-workers on the coronary artery media [62] could serve as an example of multi-scale, multi-phasic structural tissue modeling. The passive media was considered as a 3D structure consisting of helical lamellar collagen and elastin fibers interconnected by inter-lamellar elastin (Fig. 2). Structural and mechanical parameters were estimated from 3D data of inflation, extension, and twist tests under various combinations of axial force, internal pressure and torsion [63, 64]. Sensitivity analysis revealed that four parameters are sufficient to reliably represent the response under all 3D protocols (the descriptive performance—Fig. 3), and to reliably predict the tissue response under protocols not used for parameter estimation (the predictive performance—Fig. 4). These parameters are the helical angle of the lamellar fibers, two parameters of these fibers non-linear stress-strain law, and the stiffness of the inter-lamellar elastin. In a comparative study [65], this structural model out-performed earlier phenomenological and semi-structural (structurally motivated) models in both its descriptive and predictive capabilities (Fig. 5). While both the phenomenological and semi-structural models provide reasonable fit to data at certain deformation regions, they deviate from the data in other regions in both pattern and proximity to

Fig. 2 A scheme of the vessel wall media structure including the lamellae helical elastin-collagen fibers, the inter-lamellar (IL) struts, and the smooth muscle cell. From [62] with permission
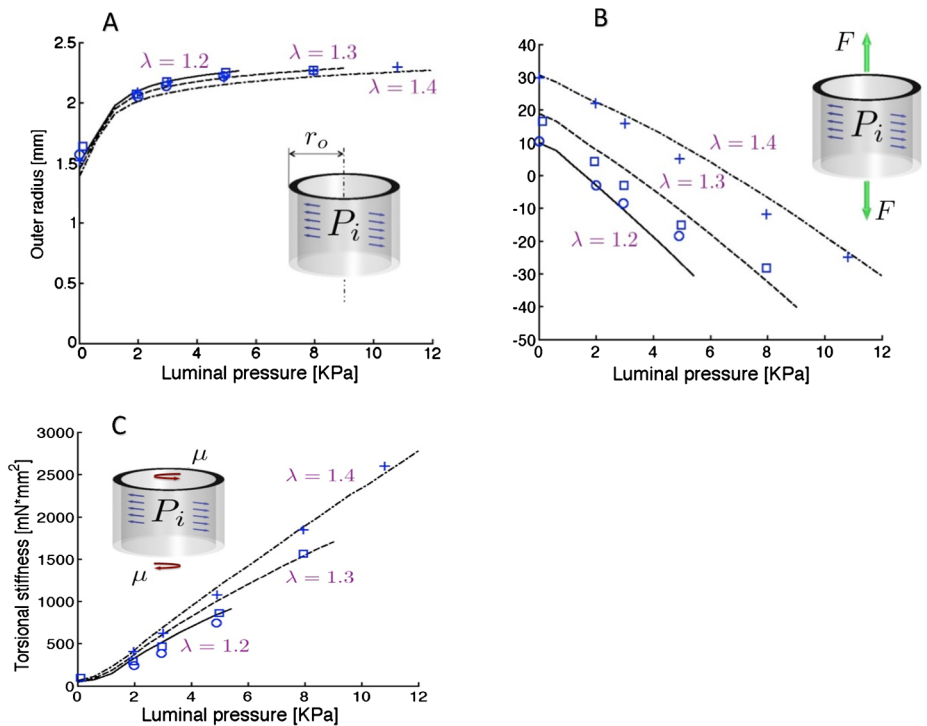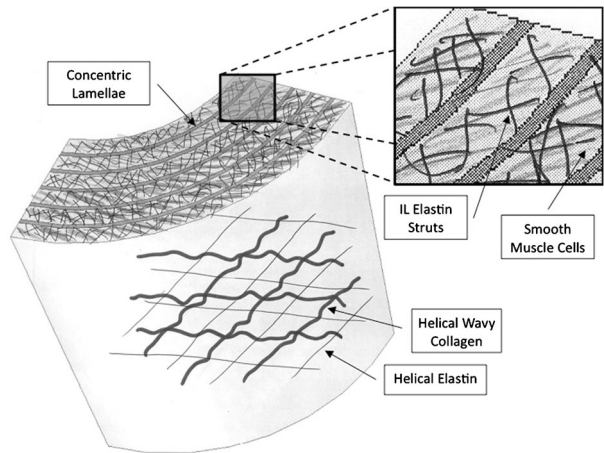

Fig. 3 The structural model descriptive power: predictions (*lines*) compared with coronary media experimental data (*symbols*) of (**A**) outer radius r_o, (**B**) axial force F, and (**C**) torsion stiffness μ, all as functions of the inner luminal pressure P_i, under three axial stretch ratios $\lambda = 1.2$ (*circle*), $\lambda = 1.3$ (*square*), $\lambda = 1.4$(+). From [62] with permission

the data. The fully structural model provided good fit under all conditions tested. Moreover, in their predictive performance, only the structural model was able to reliably predict the tissue response under protocols not used for parameter estimation.
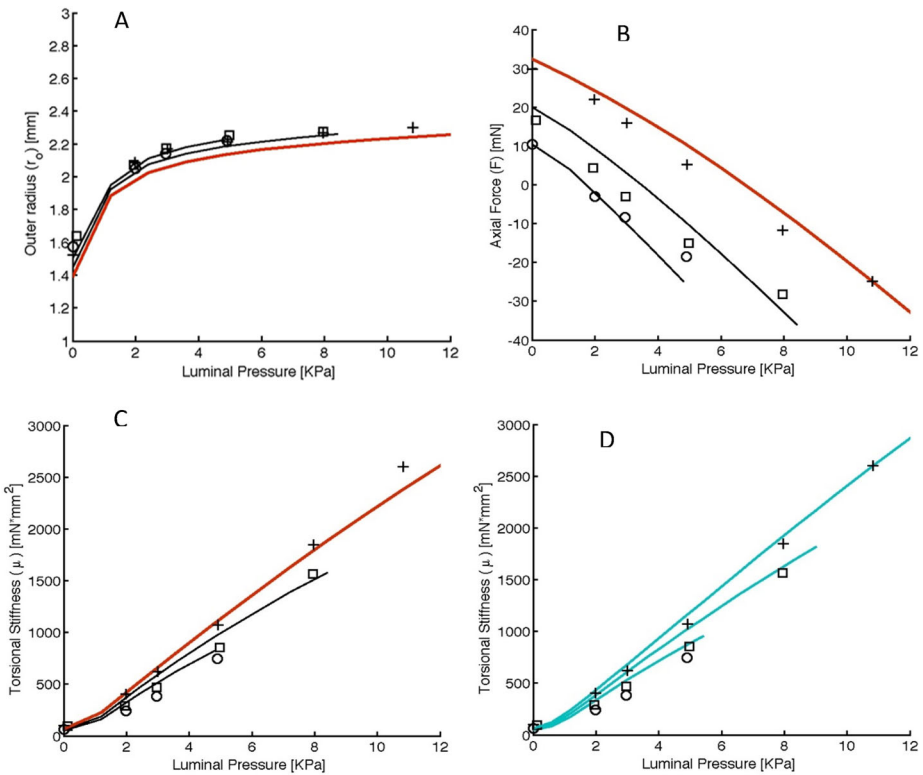
Fig. 4 The structural model predictive power: (**A**, **B**, and **C**)—comparison of coronary media data under three stretch ratios (*symbols* as in Fig. 3) with predictions using parameters estimated from partial data under stretch ratios 1.2 and 1.4 (*black lines*), and comparison with data of stretch ratio 1.3 (*red line*) not used for parameter estimation. (**D**) comparison of torsion stiffness vs. internal pressure data under three stretch ratios (*symbols* as in Fig. 3) with predictions (*blue lines*) of torsional stiffness with parameters estimated from inflation-extension data. From [62] with permission

2.8 The Matrix Osmotic Pressure

The tissue matrix consists of mobile molecules of water, anions and cations and negatively charged immobile PG macromolecules. The matrix osmotic properties arise from the thermodynamic conditions that under equilibrium (no flow of ions and water), the chemical potentials of the water in the matrix and in the external fluid must be equal. In thermodynamics the chemical potential of the water is the sum of its driving forces (the forces that can move the water) given by [66, 67]

$$\mu^w = \mu_0^w + RT \cdot \ln\left(a^w\right) + P\bar{V}^w, \tag{2.22}$$

where μ_0^w is the water reference chemical potential, which is a universal constant, a^w is the water chemical activity, P and $\bar{V}^w$ are respectively the water hydrostatic pressure and molar volume, and R and T are respectively the universal gas constant and absolute temperature. Equality of the internal and external chemical potentials of the water implies that $\mu_{mat}^w = \tilde{\mu}^w$, where the upper tilde designates external fluid. Let $\tilde{\mu}^w$, $\tilde{a}^w$, and $\tilde{P}$ be the corresponding terms of Eq. (2.22) in the external fluid, and μ_{mat}^w, a_{mat}^w, and P_{mat} in the tissue matrix. Then
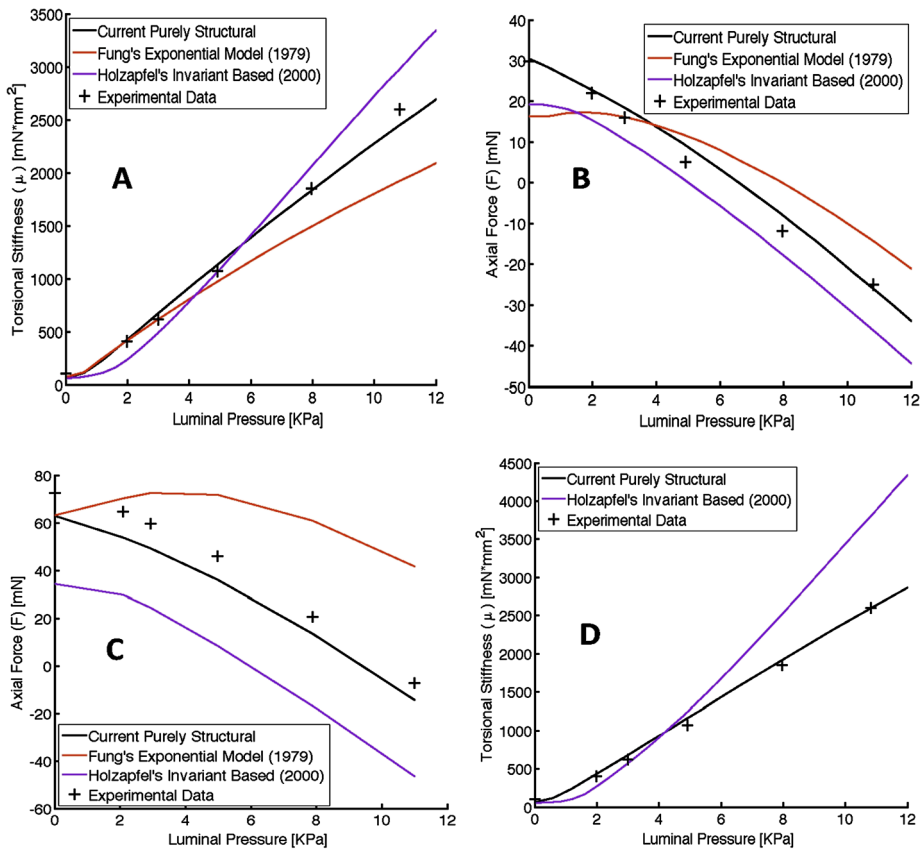
Fig. 5 Comparison of the structural model (*black line*) to Fung [144] exponential phenomenological model (*brown line*) and to Holzapfel et al. semi-structural (invariant-based) [59] model (*purple line*) by contrasting the models' predictions against 3D inflation/extension/twist response data of coronary artery media layer. (**A**, **B**) The models descriptive performance (fit to data used for parameter estimation) in predicting axial force and torsional stiffness responses, respectively, under axial stretch of 1.4 and increasing luminal pressure. (**C**) The models predictive performances (fit to data not used for estimation) in predicting the axial force under axial stretch of 1.4 and increasing luminal pressure based on parameter estimation from corresponding data under axial stretches of 1.2 and 1.3. (**D**) The models predictions of the torsional stiffness under axial stretch of 1.4 and increasing luminal pressure based on parameters estimated from 2D inflation/extension data under the same axial stretch. Fung's model torsion predictions could not be compared here since its torsional stiffness is a separate parameter that can be estimated only from twist data

by Eq. (2.22), the equality of chemical potentials implies that

$$P_{mat} - \tilde{P} \equiv \Delta P = -RT \cdot \left[\ln\!\left(a^w\right) - \ln\!\left(\tilde{a}^w\right) \right] / \bar{V}^w. \tag{2.23}$$

The water activity $-RT \cdot \ln(a^w)/\bar{V}^w$ is termed "osmotic pressure", designated by π. Equation (2.23) implies that under equilibrium, $\Delta P = P_{mat} - \tilde{P} = \Delta \pi \equiv \pi_{mat} - \tilde{\pi}$, i.e., the interior/exterior hydrostatic and osmotic pressures differences are mutually equal.

The water activity is related to its concentration by $a^w = y^w c^w$, where y^w is the water activity coefficient, which is taken to be equal in the external and internal fluids, and c^w is the water molar concentration, equal to the number of moles of water in the solution divided by

the solution volume. Insertion into Eq. (2.23) yields $\Delta \pi = -RT \cdot [\ln(c^w) - \ln(\tilde{c}^w)]/\bar{V}^w$. The presence of ions implies that the water concentration is less than one ($c^w, \tilde{c}^w < 1$), so that the osmotic pressure terms are always positive. In addition, the interior ion concentration is higher than the exterior one, since in addition to the negative free ion charges in both internal/external fluids, an excess of positively charged cations exists in the matrix fluid to counter-balance the fixed negative charges of the PGs. Higher ion concentration means a lower water concentration, so that the interior water concentration is smaller than the exterior one. This implies that both hydrostatic and osmotic pressure differences are positive, ($\Delta \pi = \Delta P > 0$).

The matrix pressure required to balance the tissue osmotic pressure difference builds up as water filtrates into the tissue, thereby swelling it and stretching the tissue fibers. In an unloaded tissue at equilibrium, two conditions are satisfied: thermodynamic equilibrium between matrix hydrostatic and osmotic pressures ($\Delta \pi = \Delta P$), and mechanical equilibrium between the fibers' stress produced by their tension, and the matrix hydrostatic pressure. Following the mixture theory [68], the total tissue stress is the weighted sum of the fibers stress and of the fluid matrix pressure (the rule of mixtures—Assumption B6). Hence, in terms of Cauchy stresses, under equilibrium, the tissue stress is the sum of all networks stresses and the matrix pressure, namely

$$\Sigma_{tiss}(\mathbf{E}) = \sum_i \left[\Sigma_{net}^i(\mathbf{E}) \right] - P_{mat}\mathbf{I}, \qquad P_{mat} = \tilde{P} + \Delta \pi. \tag{2.24}$$

2.9 The Matrix Hydrostatic Pressure

The term P_{mat} representing the hydrostatic pressure in the fluid matrix, has a clear physical meaning. Equation (2.24) has a similar form to expressions proposed in a number of previous modeling studies where the term P (instead of P_{mat} in Eq. (2.24)), is a Lagrange multiplier which arises from the constraint of tissue incompressibility. Yet soft tissues are, in general, compressible even though their constituents are incompressible. In the transition between equilibrium configurations under two different loadings, water may filtrate in or out of the tissue thereby changing its volume, until a new steady state is reached, which satisfies both mechanical and thermodynamic ($\Delta \pi = \Delta P$) equilibriums. Yet, Eq. (2.24), which results from the rule of mixtures, still holds regardless of possible volume changes. Under short loading protocols, there is insufficient time for fluid filtration and the volume changes may be negligible. The tissue can then be regarded as approximately incompressible. Under each short loading the tissue can be under mechanical but not under thermodynamic equilibrium. The pressure P can then be considered a Lagrange multiplier. Importantly however, its value is determined by the loading boundary conditions and is, in general, different from its level under both mechanical and thermodynamic equilibrium (second term in Eq. (2.24)).

2.10 Tissue Swelling and Residual Stress

Tissue swelling by the matrix pressure has a number of important consequences. First, tissues are kept well hydrated, a requisite for the cells' survival and a distinct mechanical advantage associated with the water plasticizing effect. In addition, swelling increases tissue rigidity and stiffness [69]. Un-swollen tissues (under vanishing matrix pressure) are stress-free since the fibers become un-stretched. Since they have no contraction stiffness (Assumption B4), the fibers buckle, assuming a variety of undulated configurations, and the tissue becomes floppy, showing no resistance to loading. It has no fixed stress-free nor un-loaded configurations and cannot develop residual stress [20]. Under non-vanishing matrix

pressure, the tissue swells, its fibers become stretched and the tissue acquires compressive as well as bending stiffness. Swelling and its resulting tissue stiffness lead to the onset of residual stress (RS), which carries distinct functional advantages in a number of tissues and organs.

An examination of the mechanisms of tissue RS [20] revealed that there is a hierarchy of RS producing mechanisms. At the micro-level (tissue interstitium), RS is induced by local interactions between the tissue constituents (fibers, cells, ground substance matrix). It can stem either from direct contact stresses between the tissue solid constituents, which result from their incompatible growth and remodeling [70, 71], or from the tissue swelling by the osmotic matrix. Analysis of published observations and measured data [20] suggested that under *in vivo* conditions, the osmotic driven swelling is the predominant micro RS-producing mechanism. At the meso-level, additional RS, results from internal interactions between non-homogeneities in either the tissue properties [72] or in its micro-structure and composition (e.g., between the media and adventitia in the arterial wall [73], or between sub-layers of the wall [74, 75]). The macro-level (organ) RS arises from organ-level kinematic constraints on the tissue structure which produce additional internal loading (e.g., forces and bending moments required to close the open artery from its unloaded open configuration). Based on these considerations, it was proposed that the onset of macro (OA-related) and meso (heterogeneities- related) RS depends on the presence of a micro RS. Without micro-RS, the tissue would be floppy and incapable of developing contact stresses between in-homogeneities nor bending resistance to closure of the opening angle. The crucial role of tissue swelling has been experimentally supported by the observed significant effect of os-molarity on tissue swelling and its OA level (a metric of RS magnitude) in the left ventricle, aorta and other arteries in rats [18, 73, 76], and by the finding that a true stress-free state in a carotid artery can only be reached by enzymatic destruction of the swelling-resisting elastin fibers in the media layer of the vessel wall [74]. Such destruction removes the fiber network in which the PG are encaged, thereby allowing them to exudate from the tissue space, thus abolishing the associated micro-RS and with it, the other RS components.

3 Tissue Viscoelasticity and Preconditioning

Soft tissues are not hyper-elastic but rather viscoelastic (VE). They also undergo preconditioning (PC) adaptation to loading [34]. These time-dependent response aspects are inherent properties of tissues in the sense that they significantly affect their function. Yet they are often ignored in tissue modeling. There is one important exceptional case in which tissues can be considered close to hyper-elastic: cardiovascular (CVS) tissues function *in vivo* under long-term constant cyclic loading imposed by the dynamic blood pressure. Under these circumstances, CVS tissues are fully preconditioned to their loading and, in addition, their VE is nearly exhausted, thereby demonstrating close to elastic response. In general, however, tissue VE and PC must be integrated into their constitutive formulation and failure to do so results not only in inability of the model to account for the observed time-dependent response but also in protocol-dependence of the models and their estimated parameters, thus lacking generality and reliability under general deformation schemes and losing their usefulness in analysis and design.

Previous non-elastic tissues models have addressed solely the VE aspect. Linear viscoelastic (LVE) and quasi-linear ones (QLV) models assumed that the viscoelastic stress relaxation function is strain-independent. While LVE considers a linear immediate ("elastic") stress-strain relationship (the tissue response under infinitely fast step deformation),

the widely used QLV theory [11, 34] admits non-linear immediate response in line with experimental observations. For uniaxial tissue bundles, such as in tendons and ligaments, the second Piola-Kirchhoff QLV stress is expressed as:

$$S_{bun}^{QLV}(e,t) = \int_0^t G(t-\tau) \cdot \frac{dS_{bun}^e(e)}{d\tau} \cdot d\tau = \int_0^t G(t-\tau) \cdot \frac{dS_{bun}^e}{de} \cdot \frac{de}{d\tau} \cdot d\tau, \qquad (3.1)$$

where $G(t)$ is the reduced relaxation function, and $S_{bun}^e(e)$ is the immediate bundle response.

QLV validity has been questioned and is not generally accepted. While some studies demonstrated good predictive performance of QLV, others did not. In particular, ligament creep and stress relaxation responses were found to be mutually incompatible [77]. Fung speculated [34] that the tissues' creep response may be more non-linear than its relaxation response. We proposed [78] that these disagreements stem from inadequacies in the experimental procedures used and from failure to consider the tissues dynamic structure in modeling the tissue response. For example, in some studies, samples were not fully preconditioned thereby introducing bias due to uncontrolled combination of PC and VE effects on the tissue response. This occurs since both PC and VE exhibit stress decay under repeated deformation cycles. VE and PC differ, however, in that *in vitro* VE decay is reversible after rest period, while PC effects are at least partially irreversible.

To shed light on the true nature of time-dependent tissue responses, an experimental procedure aimed to separate between PC and VE effects, was developed. The results in sheep digital tendons show that following PC of stretch cycles repeated up to a stable response, a pure viscoelastic response was subsequently obtained provided the highest strain used was 1 % lower than the strain used for preconditioning [78].

From the modeling aspect, it is natural to apply structural models for studying VE and PC, since these non-elastic features are properties of the tissue fibers. As such, they can be readily integrated into the recruiting fibers modeling in the structural approach. This can be readily seen in Eq. (2.20). The only mechanical term in this equation is the fibers' hyperelastic stress-strain law $s_f^i(e_f)$. Hence, in cases of time-dependence, the sole modification needed is to replace this term with the corresponding time-dependent term $s_f[e_f(q,t),t]$, as elaborated below.

3.1 Theory of Recruitment Viscoelasticity (RVE)

The recruitment viscoelasticity (RVE) theory was developed [78] in an attempt to reconcile conflicting observations and paradigms regarding tissue VE. It incorporates the fiber' VE in the framework of a recruiting tissue structure. Viidik [54] found that when a tendon is stretched, its non-uniformly undulated collagen fibers at reference gradually become straight with stretch while the tendon stiffness increases (the "toe" region), until all fibers are stretched and the force-stretch response becomes linear (the linear region). Unloading produces a reverse response, but is subjected to hysteresis. This suggests that the tissue fibers are viscoelastic. Assuming that their reduced relaxation function G depends solely on time and is stretch-independent, the fiber's second Piola-Kirchhoff stress is

$$s_f[e_f(q,t),t]$$
$$= \begin{cases} \int_0^t G(t-\tau) \cdot \frac{ds_f^e(e_f)}{d\tau} \cdot d\tau & \forall e_f > 0 \quad \text{(stretched fiber)}, \\ 0 & \forall e_f \leq 0 \quad \text{(buckled fiber)}, \end{cases} \qquad (3.2)$$

where $s_f^e(e_f)$ is the fiber's immediate response [11]. Replacing $s_f(e_t)$ in the recruiting bundle stress formula (2.7) by this expression, while ignoring, for now, the orientation dependence of $D(q)$, gives

$$S_{bun}^{RVE}\big[E_{bun}(t)\big]$$
$$= \begin{cases} \phi_f^0 \int_0^{E_{bun}} \dfrac{D(q)}{(1+2q)} \cdot dq \cdot \int_0^t G(t-\tau) \cdot \dfrac{ds_f^e(e_f(q,\tau))}{d\tau} \cdot d\tau & \forall e_f > 0, \\ 0 & \forall e_f \le 0. \end{cases} \quad (3.3)$$

The elastic response s_f^e depends on time solely via the fiber strain $e_f(q,t)$. Hence by chain differentiation, Eq. (3.3) assumes the form

$$S_{bun}^{RVE}\big[E_{bun}(t)\big]$$
$$= \begin{cases} \phi_f^0 \int_0^{E_{bun}} \bar{D}(q) \cdot dq \cdot \int_0^t G(t-\tau) \cdot \dfrac{ds_f^e(e_f)}{de_f} \cdot \dfrac{\partial e_f(q,\tau)}{\partial \tau} \cdot d\tau & \forall e_f > 0, \\ 0 & \forall e_f \le 0, \end{cases} \quad (3.4)$$

where $\bar{D}(q) = D(q)/(1+2q)$ is a modified fibers recruitment distribution. Equation (3.4) is the 1D version of the RVE theory.

3.2 Validity of the Recruitment Viscoelasticity Theory

Validity testing of RVE alone was carried out [78] on each specimen in order to avoid bias arising from inter-sample biological variability. The fibers' relaxation function was taken to be a three-term exponential Prony series expressed by[3]

$$G(t) = k_0 + k_1 \operatorname{Exp}\left(\frac{-t}{\tau_1}\right) + k_2 \operatorname{Exp}\left(\frac{-t}{\tau_2}\right) + k_3 \operatorname{Exp}\left(\frac{-t}{\tau_3}\right), \quad (3.5)$$

where the three terms represent respectively short, medium, and long relaxation processes. The fibers' recruitment density was assumed to be a beta function[4]. The model parameters were estimated from data of sheep digital extensor tendons, subjected to a sequence of short and long stress relaxation protocols to decreasing stretch levels of 6 %, 5 % and 4 %. RVE validity was first tested for its descriptive performance (fit to data used for parameter estimation). The results show (Fig. 6) that while in the first 6 % domain, where the tissue was not fully preconditioned, RVE fit was poor, while in the subsequent 5 % and 4 % series, during which the tissue was fully PC and the response was therefore purely VE, RVE predictions fit the data very well. Another validity test addressed RVE predictive performance (fit to data not used for parameter estimation). With parameters estimated from stress relaxation tests, the predicted creep response fit the data very well provided the stretch level remained slightly lower (by 1 %) than the PC stretch, a strain range under which there are no PC effects and the response is purely VE. Hence, the apparent previously reported incompatibility [77] of stress relaxation versus creep responses, is resolved by the structural theory. Further support of the RVE theory comes from combined VE and PC studies presented below.

---

[3]The Prony series in Eq. (3.5) is not related to the underlying mechanisms which give rise to the fiber's viscoelasticity. These mechanisms are insufficiently known. In common with other phenomenological VE models, this Prony representation is not unique.

[4]The beta function was preferred over the normal one since it is physically more realistic and more general: it is bounded, can be symmetric and non-symmetric, and can assume different shapes.
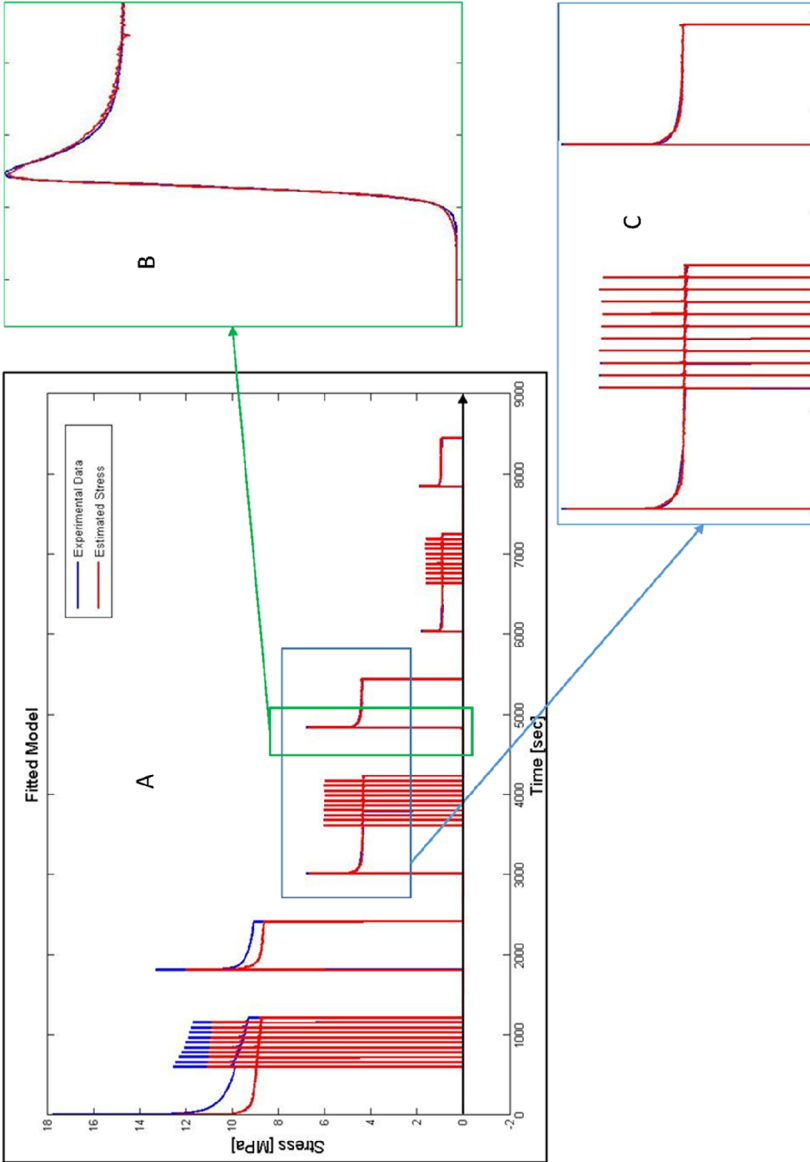
Fig. 6 (**A**) RVE descriptive performance: comparison of the tendon data (*blue line*) under a sequence of short and long stress relaxation test to stretch levels of 6 %, 5 %, and 4 % to the model predictions (*red line*). The fit is excellent under 5 % stretch where the tissue is fully preconditioned (*red and blue lines in insets* **B** and **C** are indistinguishable), but not good at 6 % stretch where the tissue is not fully preconditioned (**A**). Modified from [78] with permission

3.3 Recruitment Versus Quasilinear Viscoelasticity

Examination of the RVE relative to the QLV theory can shed light on the differences between them and elucidate the reasons for QLV success under some circumstances and failure under others. Analytically, in the RVE stress expression (Eq. (3.3)), if and only if the integrand $\frac{ds_f^e(e_f(q,\tau))}{d\tau}$ is a single-single valued function, then the order of integration can be changed so that

$$S_{bun}^{RVE}(e,t) = \int_0^t G(t-\tau) \cdot \int_0^e \frac{D(q)}{1+2q} \cdot \frac{ds_f^e(e_f(q,\tau))}{d\tau} \cdot dq \cdot d\tau. \tag{3.6}$$

By Eq. (2.7), the inner integral is equal to the time derivative of the bundle elastic response S_{bun}^e. Hence,

$$S_{bun}^{RVE}(e,t) = \int_0^t G(t-\tau) \cdot \frac{dS_{bun}^e}{dt} \cdot d\tau. \tag{3.7}$$

Equation (3.7) is identical to the QLV equation (Eq. (3.1)). However, the condition of single-single valued integrand is only valid when all fibers in the bundle are stretched. If however, some fibers contract and buckle during the stretch protocol, then their elastic stress vanishes along the entire range of negative fiber stretch, and the condition of single-single value is no longer maintained.

It is thus seen that the QLV theory is equivalent to RVE theory and is valid only if no fibers buckle during the deformation protocol. This condition is met by both creep and stress relaxation tests. Yet, under physiological conditions, the strain is likely to be dynamic and fibers are likely to contract and buckle during activity. In such cases the QLV theory is invalid. RVE, on the other hand, incorporates fiber buckling and is thus valid under general protocols. The case of quick release tests demonstrates this point. Experimentally, soft tissues which function under tension cannot support compressive load (Fig. 7). Model realization showed, however, that QLV predicts negative stress under quick release, while RVE correctly predicts zero stress (Fig. 8).

RVE can be readily generalized to three-dimensional networks as was done for the 1D case. When the fiber VE model (Eq. (3.2)) replaces the fiber hyper-elastic model in the three dimensional network stress equation (Eq. (2.14), then the following network VE stress is obtained

$$\mathbf{S}_{net}^{RVE}(\mathbf{E},t) = \phi_f^0 \int_\Omega \mathbb{R}(\mathbf{N}) \cdot \left[\int_0^{E_{bun}(\Omega)} \left[D(q,\mathbf{N})/(1+2q) \right] \cdot \int_0^t G(t-\tau) \right.$$
$$\left. \cdot \frac{ds_{fq}^e(e_f)}{d\tau} \cdot d\tau \cdot dq \right] \cdot \mathbf{N} \otimes \mathbf{N} \cdot d\Omega. \tag{3.8}$$

3.4 Recruitment Preconditioning (RPC)

Experimental observations showed that tendon PC under repeated stretch cycles is associated with increase in their unloaded reference length. Although the effects of PC *in vivo* are fully reversible, under *in vitro* conditions they are only partially reversible after a long rest. Experience has shown that in all soft tissues, PC effects are strain-dependent and have two components, one is plastic (time-independent), the other is viscous (time-dependent). It is logical to assume that since the tendon properties derive from its parallel fibers, PC in a single collagen fiber is due to increased fiber reference length, and that the PC effects have plastic and viscous components. Hence, in the structural model of sheep digital extensor
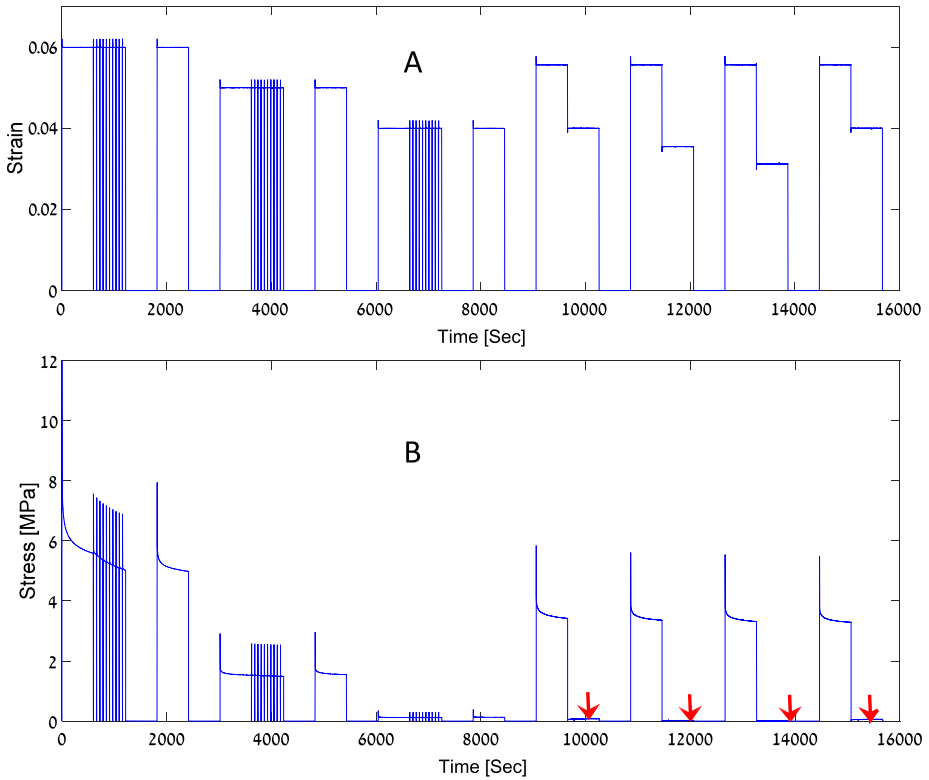
Fig. 7 Response of the fully preconditioned tendon to quick release protocols under decreasing levels of stretch (**A**). No negative stress was demonstrated in any of the tests (*red arrows* in **B**) demonstrating absence of compressive rigidity in the tissue. From [78] with permission

Fig. 8 Simulated RVE and QLV responses (**B**) to quick release to a strain e3 at which some fiber buckle (**A**). X0 is the recruitment strain of longest fiber which buckle under strain lower than x0. While QLV predicts onset of negative stress, no such stress is predicted by RVE, in line with experimental evidence (**B**). From [78] with permission
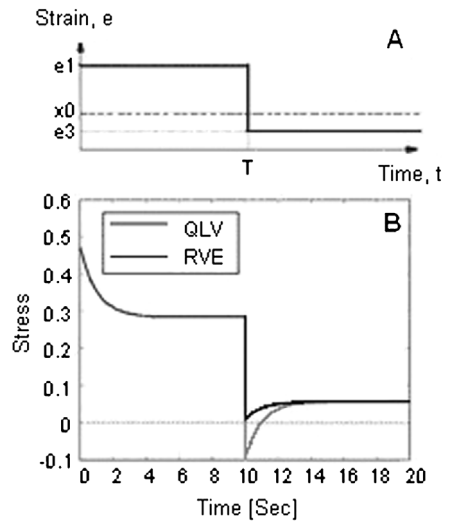
tendons, PC in collagen fibers was modeled [15] by a combination of linear viscous and linear plastic components expressed respectively by:

$$\frac{de_s}{dt} = \begin{cases} p_{1c}(e_f - p_{2c}), & e_f > p_{2c}, \\ 0 & \text{otherwise,} \end{cases} \tag{3.9}$$

$$\frac{de_s}{dt} = \begin{cases} \dfrac{de_f(t)}{dt}, & e_f > p_{3c} > 0, \dfrac{de_f(t)}{dt} > 0, \\ 0, & \text{otherwise,} \end{cases} \tag{3.10}$$

where e_s is the fiber straightening strain, p_{2c} and p_{3c} are strain thresholds below which no viscous or plastic lengthening occurs, and p_{1c} is a viscous constant. These PC laws are applied to all collagen fibers, whether they are in a uniaxial bundle or in a multi-dimensional network.

In contrast to the tendon, uniaxial skin tests showed that while PC affects the stress response at low strain levels, it has an insignificant effect on the reference length [79]. Since elastin fibers dominate the skin low strain response, it is reasonable to assume that PC affects the elastin fiber stiffness but does not increase its length. In view of its observed initial linearity (up to approximately 60 % stretch) which is followed by convex non-linearity at high strain levels, the elastin stress-strain response was taken to be a combined linear and non-linear functions of strain as in $s_e(e) = A_e \cdot e + B_e \cdot e^{Ne}$. In most studies the strain does not reach the non-linear elastic range. Hence it was assumed that PC affected the linear constant A_e, while the non-linear constants B_e and N_e, remained unchanged. The reduction of elastin stiffness from its initial (A_e^0) to its fully preconditioned (A_e^{eq}) value was assumed to depend on the fiber's highest PC strain $e_{\max}$ (the Mullins effect [80] known in rubbers and polymers), following the equation

$$A_e^{eq} = A_e^0 \big[1 + L \cdot e_{\max} + F \cdot e_{\max}^M \big], \quad L, F < 0, \tag{3.11}$$

where L, F, and M are material constants which were estimated from the data.

3.5 Validity of the Combined Preconditioning-Viscoelastic Recruitment Formulation

As discussed above in connection with hyper-elastic models, two important general validity criteria of constitutive models (model convexity and objectivity) are satisfied by hyper-elastic structural models. Assigning VE and PC properties to the fibers does not violate this validity. At each point in time, the fibers' forces are integrated to produce the tissue REV stress tensor in the same way as in the hyper-elastic case. The structural constitutive laws are thus both objective and convex also with time-dependence of the fibers properties.

Two studies have demonstrated the essential role of VE and PC in tissue constitutive formulations. One study was performed with sheep digital extensor tendons [15] which consist of a bundle of non-uniformly undulated (gradually recruiting) collagen fibers. The recruitment dispersion was assumed to follow a beta distribution. The fiber VE was modeled by RVE and their PC, by Eqs. (3.9), (3.10). The combined recruitment, PC and VE aspects were used to account for the tendon response under a sequence of short and long stress relaxation protocols at increasing (4 %, 6 %, 8 %) and then decreasing (7 %, 6 %) stretch levels (Fig. 9). Sensitivity analysis and visual inspection revealed that a remarkably good fit and very good predictive capabilities of the response under this complex protocol are

Fig. 9 The tendon composite test protocol consisting of a sequence of short and long-term relaxation tests at a constant stretch (4 % in **A**) which was then repeated at increasing (6 %, 8 %) then decreasing (7 %, 6 %) stretch levels (**B**). From [15] with permission
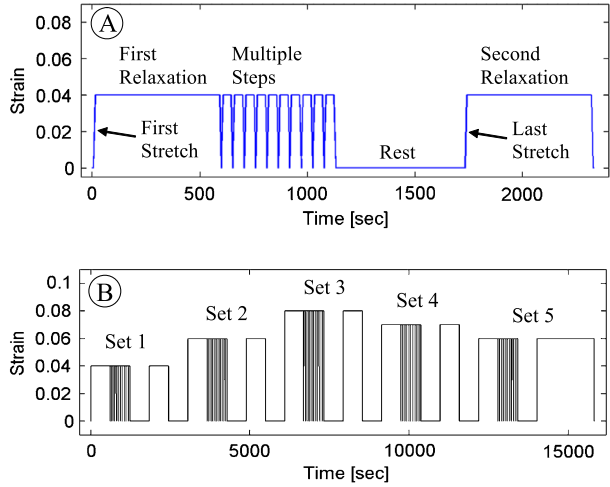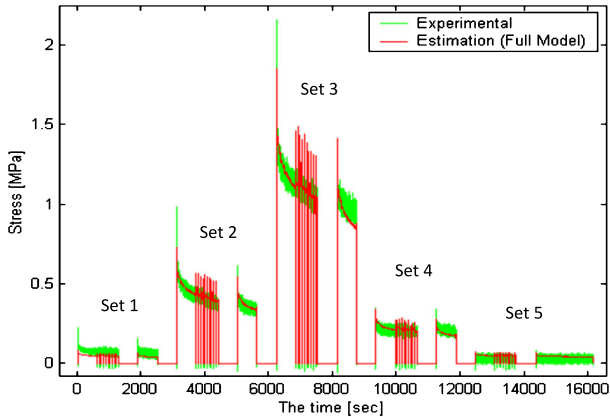
Fig. 10 Descriptive performance of the combined RVE and RPC uniaxial tendon model [15]. Comparison of data to model predictions under the protocol in Fig. 9. The model (*red line*) successfully predicts the data (*green line*), including the significant PC induced difference between the first (*Set 2*) and second (*Set 5*) 6 % response data. From [15] with permission

obtained when both collagen PC and VE features are included (Fig. 10). In another study [14], the rabbit skin non-linear and time-dependent response data [13] under various combinations of biaxial stretch protocols (Fig. 11), were modeled by a multi-fiber (collagen and elastin) structural model incorporating both the fibers orientation and recruitment dispersions. The collagen PC and VE were modeled as in Eqs. (3.5), (3.9), (3.10). The elastin PC was modeled by Eq. (3.11) and its VE by Eq. (3.5). Sensitivity analysis revealed that both elastin non-linearity (the $B_e \cdot e^{Ne}$ term) and its VE have little effect on the skin biaxial response. Comparison with measured data showed a good fit to data under all biaxial protocols (Fig. 12), and good predictive performance (Fig. 7 and Tables 4 and 5 in reference [14]) when the collagen and elastin PC and collagen VE were both included in the fibers constitutive models.

It should be stressed that the indispensable role of VE and PC in the tissue constitutive formulation is not unique to structural modeling. Tong and Fung [81] attempted to apply a non-linear hyper-elastic phenomenological model to the same skin biaxial data [13] used in the aforementioned structural study [14] and showed that the model fit well to the data of each individual protocol. However, when the constants estimated in one experiment under a specific preconditioned protocol, were used to predict the stress-strain response of the same
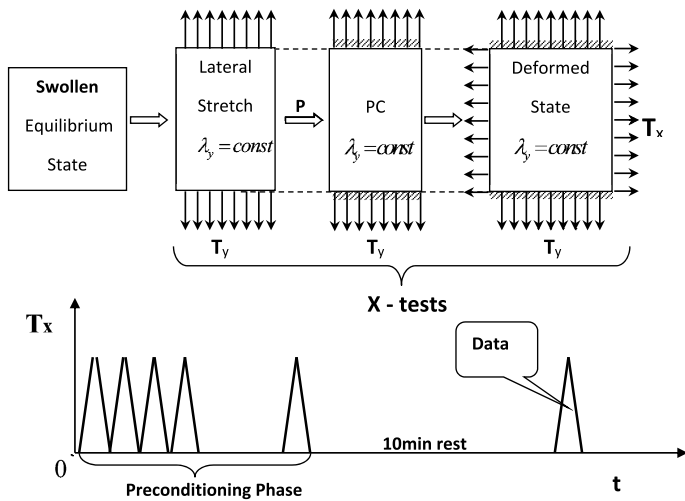
Fig. 11 The biaxial stretch protocol of a flat skin rectangular specimen [13]. In the X-tests (*upper panel*) the rectangular sample was first stretched in the lateral (Y) direction to a constant stretch, then preconditioned by repeated stretch at constant rate of stretch in the main direction (X in this test) to a set stretch level. The sample was then allowed to rest for 10 min and was then stretched to same level while data was recorded (*lower panel*). A similar protocol was applied in the Y-tests. From [14] with permission
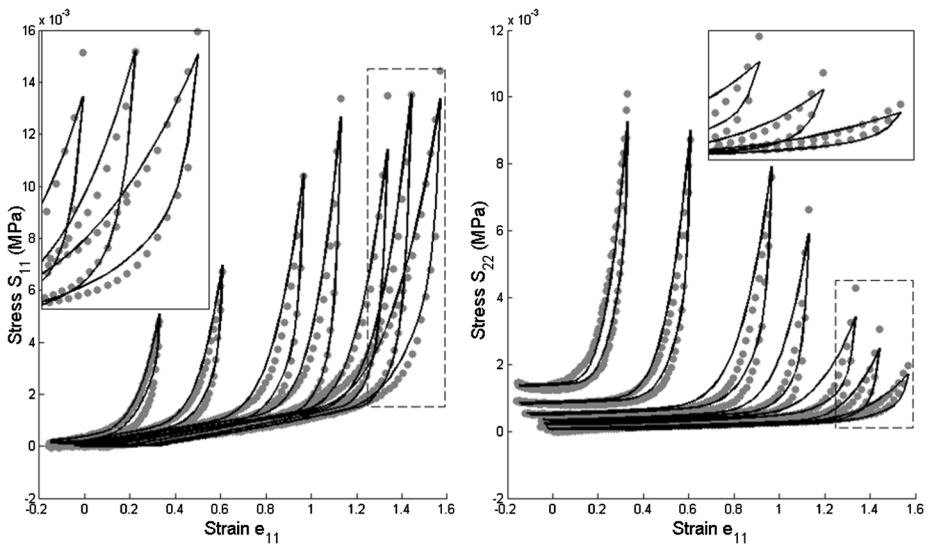

Fig. 12 Descriptive performance of the combined VE & PC biaxial structural model [14]. Comparison of skin 2D stress data under X-stretch at various fixed Y-stretch levels (*grey dots*) to model predictions (*black lines*). *Left panel*—main (X) stress, *right panel*—lateral (Y) stress responses. Predictions fit the data well for all combinations of biaxial stretches. From [14] with permission

specimen under another preconditioned protocol, success was not uniform. They concluded that since the estimated model parameters changed from one experiment to another, the tissue is not elastic. Similar inter-protocol parameter variations were observed in a variety of soft tissues (e.g., [82–86]) again demonstrating that they are not elastic.

4 Structural Modeling of Active Tissues

Multi-scale structural modeling can readily incorporate active contraction of muscular fibers and cells. The active muscle properties are subject of most extensive research published in many journals and a large number of dedicated books. In spite of substantial progress over several decades, there are still no generally accepted models for all muscle types. In general, the active muscle force depends on its length, contraction velocity, time of activation, and muscle contractility (inotropic state). But the specifics vary greatly between both the three muscle types and locations in the body. A review of this vast topic is outside the scope of the present report. Instead, the approach here is to use the framework of the structural theory, assume that the active force model of a given single muscle cell is known, and indicate the generic manner by which it is integrated and summed up with the contributions of the passive constituents in the muscle to produce the total muscle stress.

The myocardium serves here as an example. Reviews of myocardial modeling in general, and on application of constitutive models in three dimensional stress analysis of the heart, have been presented in Yin [87] and more recently by Glass et al. [88] and Schmid and Hunter [89].

Activated muscle fibers (such as in skeletal muscle) apply contraction force in their axis direction. Muscle cells (myocytes and smooth muscle cells) contract along the direction of their sarcomere which usually coincides with their long axis.

4.1 Myocardium Structure

The myocardium is a fibrous tissue in which the myocytes occupy about 70 % of the volume while the remaining ∼30 % is occupied by the fluid matrix (∼20 %), other types of cells (e.g., fibroblasts) and other interstitial components [90]. Collagen fibers occupy only about 5 % of the weight [91] but are an important determinant of the tissue passive properties [92]. Light microscopy (LM) images showed that the left ventricle (LV) wall structure is both locally anisotropic and heterogeneous across the wall thickness. The myocytes are elongated cells arranged in a layered disposition and parallel to each other with a circumferential angle (Γ in Fig. 13) which varies gradually from the inner endocardium to the outer epicardium wall surfaces [93]. Longitudinally, myocytes are interconnected via dense intercalated discs which provide the cells with mechanical, electrical and chemical inter connections, thereby

Fig. 13 Scheme of the parallel myocytes orientation distribution across the myocardial wall and of the transverse collagen network interconnecting neighboring myocytes (*inset*)
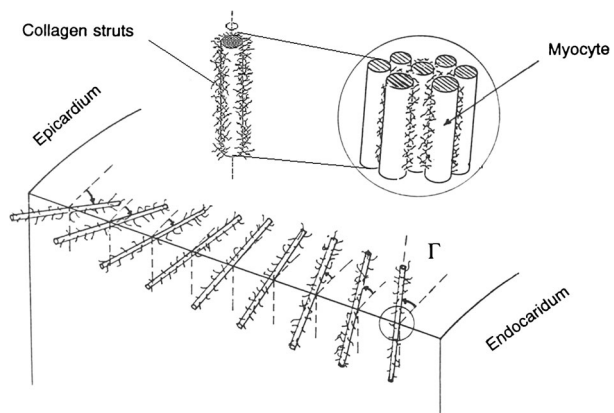
forming fiber-like structures and facilitating functional integrity as a syncytium. Scanning electron microscopy (SEM) images demonstrated that the collagen component forms both crisscross weaves which surround individual or groups of myocytes, and a dense array of transverse collagen struts which interconnect contiguous myocytes [94–97], thereby maintaining structural integrity of the myocardium.

4.2 Mechanics of the Passive Myocardium

Based on LM and SEM observations [93, 94, 96–98], a hyper-elastic structural model was developed for the passive myocardium [99, 100]. It contains an ensemble of REVs, each representing a local structural unit consisting of a single myocyte, symmetrically interconnected with its neighbors by a 3D network of initially undulated transverse collagen fibers (Fig. 13). In addition, each REV incorporated a system of passive fibers running parallel to the direction of the myocytes, representing the longitudinal contribution of the crisscross fibrous weaves which surround the myocytes, combined with that of the passive inter-myocytes titin filaments which run along the sarcomeres and the myocytes long axes [101]. Structural characterization of the myocardial wall entails specification of the orientation distribution of the transmural myocytes [93], the orientation distribution of the transverse collagen fibers relative to their REV myocyte to which they are connected, and the recruitment distribution of the collagen fibers. With these structural attributes specified, the strain field in each REV across the wall and the strain in each collagen fiber in the REV system were evaluated [99, 100] from the global myocardial strain field, based on affine deformation (Assumption B5). The passive stress in each fiber was then calculated from its strain. By the rule of mixtures, the sum of passive contributions of all transverse and parallel fibers was calculated and assigned as the overall myocardial passive fibers stress.

4.3 Mechanics of the Active Myocardium

The active stress of the myocardium results from and is equal to the sum contributions of all its myocytes. In the framework of structural modeling, the law governing the development of the active myocyte tension is assumed to be known and is a given input to the model. The active tension in each myocyte acts along its length. Stress summation across all myocytes is performed after each myocyte stress is mapped to a common global coordinate system. The resultant global active stress is then added to the global passive stress and the matrix pressure to yield the total myocardium stress.

Myocyte activation is a complex event affected by a number of determinants. The generated active force depends on external determinants (length, velocity and electric excitation), as well as on internal factors such as the kinetics of both the actin-myosin cross-bridges and of troponin and Ca^{+2} ions, which control cross-bridge attachment, and on cellular control mechanisms. A number of models have been proposed, each highlighting different aspects of the activation event. However, regardless of the model chosen, the generality of the structural approach allows any model to be integrated into the stress analysis. As a simple example, an active stress law of the form

$$\sigma_{mus}^{act}(\tau, t) = \sigma_{\max} \cdot T(\tau) \cdot L(\lambda_{mus}) \cdot V(v) \tag{4.1}$$

was used [100] in LV stress analysis along the entire cardiac cycle (diastole and systole), where $\sigma_{\max}$ is the highest possible active stress under optimal muscle stretch, $T(\tau)$ is an activation function of the time τ passed since the myocytes were activated, $L(\lambda_{mus})$ is a

function of muscle stretch, representing the dependence of the stress on the sarcomeres actin-myosin overlap, and $V(v)$ is a velocity function which reflects the hyperbolic relationship between active stress and the shortening velocity [102]. Equation (4.1) was applied to each sarcomere, then mapped to the global myocardium coordinate system and summed up across all REVs. Details on the realization and comparison of the model predictions to the LV pressure-volume data along the entire cardiac cycle are given in reference [100].

5 Multi-scale Modeling of Tissue Growth and Remodeling (G&R)

Living tissues are unique in their ability to adapt to altered mechanical environments by changing their size, shape, structure, and mechanical properties. This adaptation, termed Growth and Remodeling (G&R), occurs not only during growth, but also in adulthood in response to physical activity, pregnancy, dietary changes and pathologies, such as hypertension. There is strong experimental support to the notion that G&R results from the tissue cells' strive to maintain a homeostatic mechanical environment required for survival and proliferation (e.g., [29]). The cells do so by adapting their extra-cellular fibrous matrix (ECM) via turnover—degradation of some fibers and production and deposition of new ones.

G&R models are useful not only in providing a coherent framework and facilitating insight into the underlying processes occurring in health and under pathological conditions, but also due to their key role in tissue engineering in design and fabrication of biological constructs. For example, mechanical conditioning was found not only to stimulate matrix production but also to be a major determinant of the construct evolution towards target structures and properties [103–105].

Previous G&R models can be classified into three categories: early phenomenological models focused on the consequences of G&R, based on classical continuum mechanics. In arteries for example, G&R is manifested globally by changes in diameter and wall thickness in an attempt to maintain homeostatic wall hoop strain and luminal wall shear stress [106–109]. The constraint mixture approach was later developed [110] to facilitate separate monitoring of the evolution and contribution to the global response of each of the tissue constituents. Structure-motivated models considered the G&R-induced evolution of specific structural features such as the helical angle of collagen fibers in arterial media. Other tissue constituents (such as the media elastin and matrix) were phenomenologically modeled. A common characteristic of previous G&R models is their ad-hoc assumptions as to the phenomenology of G&R-associated geometrical or structural alterations. Alternatively, since tissue properties derive from their constituents, it is advantageous to analyze G&R in terms of the specific turnover processes experienced by each constituent in the tissue space, based on the constituent's loading history and its specific mechano-biological nature (the mechanistic approach [111]). The structural multi-scale framework presented here is highly suited for this goal, since it incorporates and monitors the mechanical environment and resulting mechano-biological turnover of each constituent, everywhere in the tissue space, and then integrates the effects of all these local events to predict the evolution of the tissue structure and associated properties. To demonstrate this approach, the case of tissues with one type of uni-directional bundle of fibers (e.g., collagen in tendons and ligaments) will be formulated in detail [112]. This will be followed by generalization to tissues with multiple types of fibers.

5.1 Basic Assumptions of the Structural G&R Theory

The multi-scale tissue G&R theory is based on similar assumptions that underlie the multi-scale theory of inanimate tissue mechanics, supplemented with the following mechano-biological assumptions regarding constituent turnover:

Assumption GR1 The characteristic time of tissue loading (seconds to hours) is several orders of magnitude shorter than the characteristic time of G&R-related biological processes (weeks to months [111]). Hence at any G&R time, the tissue response to short loading can be analyzed independent of ongoing G&R processes.

Assumption GR2 Fibers turnover occurs through degradation of some fibers while others are synthesized and deposited.

Assumption GR3 The biological processes of fiber degradation and synthesis are first-order reactions.

Assumption GR4 The reaction rates are specific to each constituent and have both loading-independent (basal) and loading-dependent components.

Assumption GR5 Synthesized fibers are deposited on extant fibers, under a stretch within the homeostatic range.

Assumption GR6 During G&R the fibers and matrix volume fractions are maintained at constant levels [70, 113].

The detailed theory formulation is laid down in reference [112]. A brief review of the main features is presented here.

5.2 The Tissue and Fiber Kinematics

The growth-induced evolution of the tissue structure, combined with tissue swelling under the matrix pressure, introduce multiple reference and loaded configurations, which are interrelated by corresponding mappings (Fig. 15). During G&R, the uniaxial tissue (Fig. 14) is progressively stretched from its original unloaded reference length $L_{tiss}^{UL}(0)$ to its growth induced length $L_{tiss}^{GR}(t)$ by a growth protocol $\Lambda_{tiss}^{GR}(t)$ which is an input to the model. The fiber bundle is simultaneously stretched from its original stress-free reference length $L_{bun}^{SF}(0)$, by an associated bundle stretch $\Lambda_{bun}^{GR}(t)$. Due to fiber turnover, growth induces changes in both the unloaded tissue and stress-free bundle reference configurations ($L_{tiss}^{GR}(t)$ and $L_{bun}^{SF}(t)$, respectively). The ratio between the tissue growth-induced length $L_{tiss}^{GR}(t)$ and its remodeling-induced unloaded reference length $L_{tiss}^{UL}(t)$ is the pre-stretch $\Lambda_{tiss}^{PS}(t)$. Finally, at each configuration during growth the tissue and bundle lengths are interrelated by the corresponding osmotic induced tissue swelling Λ_{tiss}^{osm}.

Importantly, of the several mappings between the various tissue and bundle configurations, only two are given inputs to the model, namely the tissue growth protocol $\Lambda_{tiss}^{GR}(t)$ and its short testing protocol $\Lambda_{tiss}^{test}(\tau)$. The initial tissue swelling $\Lambda_{tiss}^{osm}(0)$ is determined from the assumed initial bundle configuration and the matrix pressure. The other mappings ($\Lambda_{tiss}^{GR\ osm}(t)$, $\Lambda_{tiss}^{ref\ osm}(t)$, $\Lambda_{tiss}^{PS}(t)$, $\Lambda_{bun}^{PS}(t)$) can be evaluated only after the G&R-remodeled

Fig. 14 A scheme of the uniaxial tissue structure with its fluid-like matrix and non-uniformly undulated fibers. Only stretched fibers are stressed. From [112] with permission
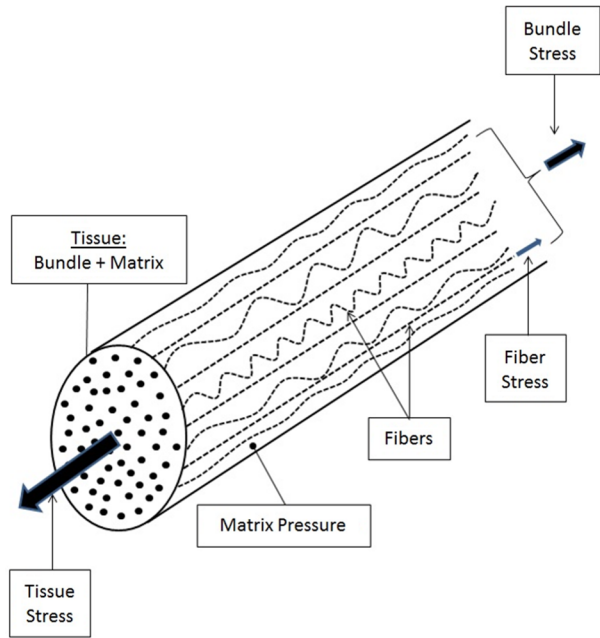
bundle stress-free configuration $L_{bun}^{SF}(t)$ has been determined from the turnover-induced evolution of the bundle structure.

The various tissue and bundle mappings are interrelated by multiplicative decomposition only when the tissue configuration (structure and composition) is fixed. For example, the bundle and tissue test stretches are inter-related by (Fig. 15):

$$\Lambda_{bun}^{test}(t^*, \tau) = \Lambda_{tiss}^{test}(t^*, \tau) \cdot \Lambda_{tiss}^{ref\ osm}(t^*), \tag{5.1}$$

where $\Lambda_{tiss}^{ref\ osm}(t^*)$ is the tissue swelling under the matrix pressure in the remodeled configuration at the test time t^*. In contrast, tissue configurational changes which include growth cannot be prescribed by multiplicative decomposition of the deformation gradients since growth itself, which involves mass changes, cannot be represented by a corresponding deformation gradient as $\mathbf{F}^\mathbf{G} = \partial \mathbf{x}^\mathbf{G}/\partial \mathbf{X}^\mathbf{G}$ [114]. Such representation implies that the coordinates of each material point prior to $(\mathbf{X}^\mathbf{G})$ and following $(\mathbf{x}^\mathbf{G})$ growth are inter-related by bijective motion (one-to-one and onto). Bijective motion is not valid for G&R during which some fibers are degraded and new ones are produced since such fibers do not have both $\mathbf{X}^\mathbf{G}$ and $\mathbf{x}^\mathbf{G}$ coordinates.

The bundle fibers are variably stretched with the tissue depending on each fiber "birth" length l_f^b, or its nominal birth stretch $\lambda_f^b = l_f^b/\Lambda_{bun}^{SF}(0)$. The birth stretch determines the true fiber stretch (which in turn determines its tension and its contribution to the tissue stress). The fiber true stretch is given by

$$\lambda_f(\lambda_f^b, t) = \Lambda_{bun}^{nom}(t)/\lambda_f^b. \tag{5.2}$$

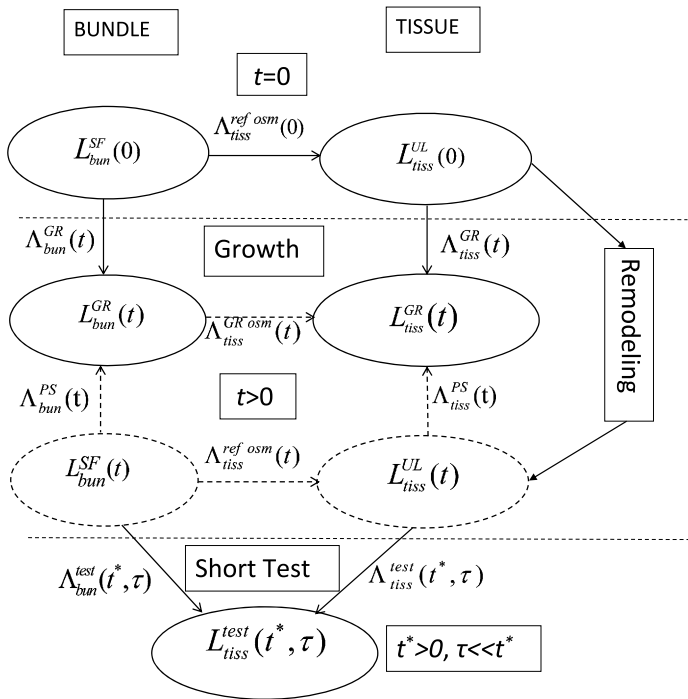Hence, although the bundle and its fibers global deformations are affine, the fibers true deformations are not.

Fig. 15 A scheme of the evolving bundle and tissue stress-free (*SF*), unloaded (*UL*), growth-induced (*G&R*), and test-loaded (test) configurations and of the mappings between them. Λ_{tiss}^{*osm} designate the tissue swelling under the matrix osmotic driven pressure. L_{bun}^{GR}, L_{tiss}^{GR} stand for the bundle and tissue growth induced dimensional changes, and $L_{bun}^{SF}(t)$, $L_{tiss}^{UL}(t)$ are the remodeled bundle stress-free and tissue unloaded configurations, respectively. Λ_{bun}^{PS}, Λ_{tiss}^{PS} are the bundle and tissue growth induced pre stretches. Λ_{bun}^{test}, Λ_{bun}^{test} are short test protocols aimed to monitor the evolution of the mechanical properties

5.3 Volume and Mass

The total fiber and matrix volumes are respectively $V_f(t)$ and $V_{mat}(t)$. The corresponding volume fractions are $\phi_f(t) = V_f(t)/V(t)$ and $\phi_{mat}(t) = V_{mat}(t)/V(t)$, where $V(t)$ is the total tissue volume. Since there are no voids (Assumption B2), then $V(t) = V_f(t) + V_{mat}(t)$, and $\phi_f(t) + \phi_{mat}(t) = 1$. Since the volume fractions remain constant during G&R (Assumption GR6 [70, 113]), it follows that $\phi_f(t) = \phi_f(0) \equiv \phi_f^0$, and likewise for the matrix.

The evolving distribution of fiber mass over its birth stretch is $m(\lambda_f^b, t)$ such that at time t the mass of fibers with birth stretches between λ_f^b and $\lambda_f^b + d\lambda_f^b$ is $m(\lambda_f^b, t) \cdot d\lambda_f^b$. The total fiber mass is therefore $M_f(t) = \int_0^{+\infty} m(\lambda_f^b, t) \cdot d\lambda_f^b$. The distributions of fibers mass and volume are interrelated by $m(\lambda_f^b, t) = \rho_f \cdot v(\lambda_f^b, t)$ where ρ_f is the fiber mass density.

5.4 Turnover Kinetics

Both fiber degradation and production are first-order reactions where each has deformation-dependent and deformation-independent components (Assumptions GR3 and GR4). The

corresponding equations for the degradation are

$$\frac{\partial^{dd} m_f}{\partial t}(\lambda_f^b, t) = -B^{dd}(\lambda_f) \cdot m_f(\lambda_f^b, t), \qquad \frac{\partial^{db} m_f}{\partial t}(\lambda_f^b, t) = -B^{db} \cdot m_f(\lambda_f^b, t), \quad (5.3)$$

where $\partial^{dd}/\partial t$ and $\partial^{db}/\partial t$ are respectively, the deformation-dependent and deformation-independent degradation time derivatives. $B^{dd}(\lambda_f)$ and B^{db} are the corresponding reaction rate constants. Similar equations hold for fiber production with corresponding rate constants $B^{pd}(\lambda_f)$ and B^{pb} where the indices pd and pb designate respectively, the deformation-dependent and basal production rate constants.

5.5 Fiber and Bundle Mechanics

Cauchy stress in a single hyper-elastic fiber is $\sigma_f(\lambda_f)$, where the fiber true stretch at time t $\lambda_f(\lambda_f^b, t)$ depends on its birth stretch (Eq. (5.2)). In the model realization, the fiber stress-strain relationship is taken to be linear, i.e., $\sigma_f = K(\lambda_f - 1)$, where K is the stiffness. The bundle Cauchy stress Σ_{bun} is the weighted sum of all the fiber contributions

$$\Sigma_{bun}(t) = (\Phi_f(t)/M_f(t)) \cdot \int_0^{+\infty} m_f(\lambda_f^b, t) \cdot \sigma_f(\lambda_f) \cdot d\lambda_f^b, \qquad (5.4)$$

where $\Phi_f(t)(= \Phi_f^0)$ transforms the stress from its level per bundle unit area to its level per tissue unit area. By the rule of mixtures, the total tissue Cauchy stress is

$$\Sigma_{tiss}(t) = \Sigma_{bun}(t) - P_{mat}. \qquad (5.5)$$

Equation (5.4) cannot be used as it stands, since at a given growth time t the fibers' birth stretches and their distribution are unknown. The experimentally measurable quantity at growth time t is the distribution of the fiber recruitment stretches $D(x, t)$, which plays a key role in the multi-scale modeling of inanimate tissue mechanics presented above[5]. It can be readily shown [112] that the distributions $m(\lambda_f^b, t)$ and $D(q, t)$ are interrelated by

$$D(q, t) = \Lambda_{tiss}^{ref} \cdot m_f(\lambda_f^b, t)/M_f(t). \qquad (5.6)$$

5.6 Feasibility of the Multi-scale Structural G&R Theory

To demonstrate the feasibility and utility of the multi-scale structural G&R theory, a specific case [112] of a uniaxial tissue whose linear elastic fibers were initially straight and un-stretched, was analyzed. The tissue was subjected to a growth protocol of a constant stretch rate of 0.5 per year for a period of two years. Kinetic and mechanical parameters values were adopted from published data. Figure 16 depicts the predicted evolution of the tissue structure in terms of fiber recruitment stretch distribution. The initial uniform distribution evolves rapidly to a bell shaped form, with no trace of the initial uniform distribution after approximately 5 % of the total growth time. The bell shaped recruitment stretch distribution is a commonly observed feature of soft tissues [53, 115–118]. The predicted tissue stress-strain response evolves from an initial linear relationship of the uniformly stretched fibers to a convex non-linear response, in which the tissue stiffens with strain (Fig. 17). Again, this feature is common to all soft tissues. A third observed characteristic is the onset of pre-strain and associated pre-stress which evolve with growth (Fig. 18).

---

[5] $D(q, t)$ has the same physical meaning at a given growth time t as the function $D(q, \mathbf{N})$ in Eq. (2.5) in a uniaxial fiber network (no dependence on $\mathbf{N}$).

Fig. 16 Evolution with growth time of the fibers recruitment stretch density distribution. Fibers having recruitment stretch lower than unity are already stretched in the unloaded length thereby balancing the matrix pressure. The symbol "*tf*" stands for the total growth period duration. From [112] with permission
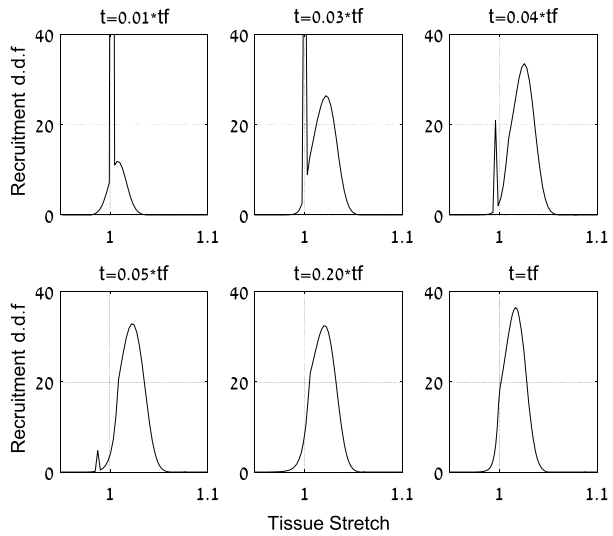

Fig. 17 Evolution of the tissue (fibers and osmotic active matrix) stress-strain relationship at selected growth times of $t = 0(+)$, $t = 0.05 * t_f$, $t = 0.08 * t_f$, $t = 0.20 * t_f$, $t = t_f$ (t_f being the duration of the growth period). (**A**) The tissue first Piola-Kirchhoff stress as function of its stretch. (**B**) The corresponding tissue total force. The initial linear response (at $t = 0$) of the uniformly straight fibers, evolves with growth time to convexly non-linear ones. From [112] with permission
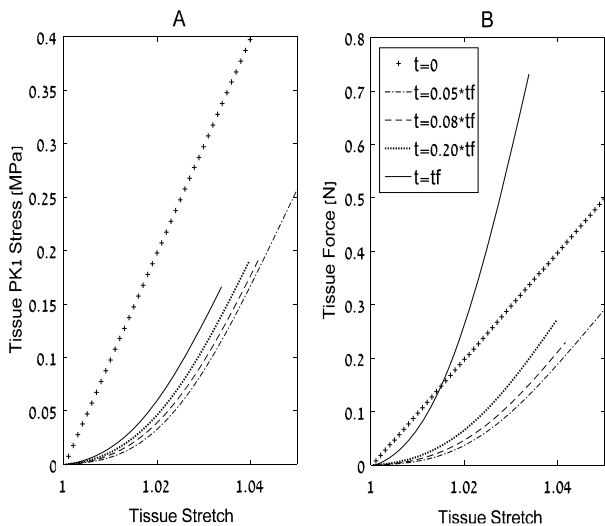
5.7 Evolutionary Determinants of Tissues Structure and Mechanics

Scientifically, it is both intriguing and of potential practical importance to determine if the evolutionary attributes of tissue structure and mechanics which are depicted in Figs. 16–18 are genetically determined. The results presented here show that these characteristics could well evolve as a result of the mechano-biology of the tissue constituents. It is shown that based solely on the turnover processes of the constituents, these three key characteristics of structure and mechanics evolve with growth towards their observed patterns.

Fig. 18 Evolution with growth time of the in situ tissue pre-stress (**A**) and pre-stretch (**B**). From [112] with permission
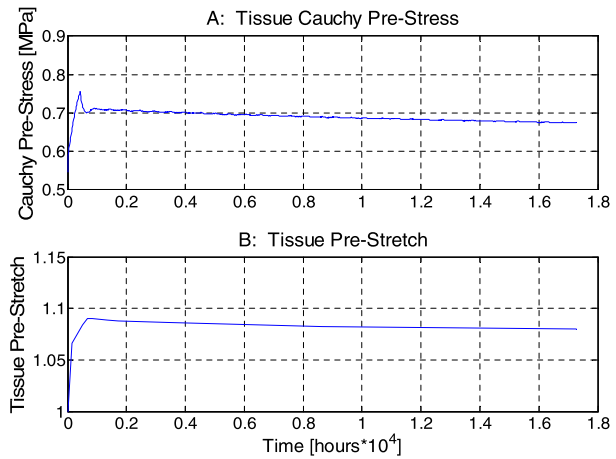
6 State of the Art, the Big Picture, Future Challenges

To summarize, an account will be given of the main merits and limitations of the multi-scale structural tissue modeling. This will be followed by a personal outlook regarding tissues characterization, along with future research challenges and prospects in the field.

6.1 Merits of the Multi-scale Structural Approach

The structural theory is of a physical nature, in the sense that it simulates real processes occurring in realistic tissue structures. The theory parameters have clear physical meaning and can often be measured independently using methodologies unelated to tissue mechanical testing (e.g., testing of individual fibers, histological staining and ultrastructural imaging). The structural approach can readily incorporate contributions of tissue constituents which are very different in their nature (e.g., fluid matrix, passive and active solid fibers) and integrate all into a clear and precisely orchestrated global tissue response. Due to its physical nature, the theory is free of the problem of indistinguishability between candidate non-linear models which is often encountered in non-linear phenomenological characterization. Moreover, and probably for the same reason, experience has shown that the inter-specimen variance between parameter estimates of structural models is significantly lower than in phenomenological models. Another useful feature of structural models is their aforementioned guaranteed physical plausibility. In terms of reliability and fit to data, detailed comparison [65] revealed that structural models are superior to non-structural models both as descriptors and predictors of 3D response characteristics of coronary arteries media. Most importantly, structural models have the unique ability to expand by smoothly incorporating additional tissue constituents with different properties, or more complex properties of constituents, such as fiber non-linearity, time-dependence, active contraction and mechano-biological turnover. It was shown above that perplexing dilemmas in tissue characterization, such as the apparent incompatibility between viscoelastic stress relaxation and creep responses [77, 78], the ranges of validity and interplay between preconditioning and viscoelasticity [78], and the

kinematic limitations and physically unrealistic response predictions occasionally encountered with nonstructural models [60, 119], can be readily resolved using structural modeling.

6.2 Limitations of the Multi-scale Structural Approach

It has been claimed that implementation of the structural approach in finite element stress analysis, presents an excessively heavy computational load due to the need to integrate the contributions of fibers over their entire recruitment stretch distribution and 3D orientation dispersion. Various attempts have been made to circumvent this problem but, so far, none have proven to reliably represent tissue response characteristics under any general loading (see discussion below in "Reduced Structure Representation"). On the other hand, in practice, with today's powerful fast mainframes and parallel coding interfaced with computer clusters, the computational load is tractable, as shown for the complex case of 3D finite element analysis of the LV with passive and active myocardium in a real geometry model [120].

Another concern raised is that by assuming deformation affinity, interactions between tissue fibers are not considered in structural models [3]. Two recent studies directly addressed this issue by experimentally testing deformation affinity [52, 58]. The results show that in the flat tissues tested (pericardium, aortic valve leaflet and mitral valve anterior leaflet), the fiber kinematics was affine. As the authors correctly conclude, affinity suggests that the fibers are largely non-interacting and deform with the bulk tissue.

6.3 The Big Picture

The research in tissue mechanics has been dominated in the past almost exclusively by phenomenological models within the powerful frame of classical continuum mechanics of bulk materials, using concepts and paradigms adopted from this discipline. Biological aspects were often adapted to fit continuum framework. Phenomenological models served as a starting point and contributed significantly to progress in tissue mechanics. However, in recent years, it is becoming clear that soft tissue characterization requires a frame of thinking that transcends the scope of continuum mechanics. The paradigm should be to model tissues based on the real structures and biological processes occurring in the tissue system, and to link the resulting formulation to continuum mechanics.

A number of reasons underlie this need for paradigm change. First, tissues are multi-scale, multi-phasic structures, exhibiting complex time-dependent responses. In addition, tissues are thermodynamically open, rather than closed systems. In the living tissue, mass, energy and information are constantly exchanged with the environment, and with the whole body. Muscle tissues are excitable and develop active contractions. All *in vivo* tissues change via biological processes, to adapt to their external environment. Hence, tissues do not fit the standard requirements of continuum mechanics. For instance, classical conservation laws are only valid in living tissues for short time periods and under passive states, but are generally violated. For one or more of these reasons, phenomenological models have proven to be limited in their ability to reliably represent the complex properties of live tissues under general conditions and deformation schemes.

It is thus submitted that future prospects in tissue biomechanics research requires a new paradigm. For tissues *in vitro* much progress has been achieved by moving from phenomenology to structure-function and casual connections. In live tissues, there is a need to expand the outlook to bodies which remodel via biological processes. These changes will require massive experimental effort to elucidate hitherto unknown features of tissue

mechano-biology and to develop testing protocols suitable for reliable model validation. While preliminary steps have been taken, much remains to be done.

From the modeling aspect, the multi-scale structural approach presented here is a platform suitable for realizing this new paradigm. On the one hand (as shown above), it can incorporate biological effects and resulting changes in mass, structure and properties. On the other hand, it bridges between the mechano-biological processes and continuum mechanics in a coherent manner. It thus affords clearer and richer insights and opens new possibilities in a significantly wider horizon compared to continuum models of inanimate materials.

6.4 Future Challenges

The realism and versatility of multi-scale tissue characterization pave the way for future research challenges, both theoretical and experimental, several of which are presented here.

Experimental Structural Characterization: Tissue structure is the cornerstone of the structural approach. In the absence of pertinent information, previous structural characterizations were for the most part indirect. Based on qualitative histological observations, general forms of orientation and waviness distributions (such as the beta function) were assigned to both features, and parameters of these distributions were estimated to best fit given mechanical response data. Attempts to directly determine the distribution functions based on morphological observations, have been impeded by difficulties in reliable extraction of the tissue 3D structural features, and by the inherent experimental uncertainties associated with the need to process the specimen, or by the use of differential digestion, thereby distorting the tissue's micro-structure. Recent developments in non-linear optics (e.g., multiphoton microscopy and coherent anti-Stokes Raman scattering microscopy), coupled with computer-interfaced sequential optical sectioning, hold great promise for 3D structural characterization. The advantage of these methodologies is that tissue samples are maintained in their native state (i.e., unstrained and unprocessed). In addition, the application of two types of nonlinear laser/tissue interaction—two photon excited fluorescence (TPEF) and second-harmonic generation (SHG),—allow for retrieval of distinct structural data for the elastin and collagen type I fibers [121, 122], respectively.

Reduced Structure Representation: Implementation of the structural approach in finite element stress analysis presents a heavy computational load due to the associated need to integrate the contributions of fibers over their entire 3D orientation distribution function (also termed "integration on a sphere"). Although modern fast computing facilities render this task tractable (e.g., in the case of the left ventricle [120]), attempts are being made to develop a computationally more efficient representation. Although promising first steps have been made, a methodology which is general enough to incorporate any tissue structure and any fiber material law is still lacking. The quest for such representation is a challenging theoretical/numerical undertaking. One current approach relies on application of generalized structural tensor to represents the tissue's 3D structure [123, 124], instead of the fiber orientation distribution. Higher computational efficiency was achieved with the structure tensor since in application, it was multiplied by a weighted average of the fiber stretches, thus ignoring dependence of the latter on the fiber orientation. Comparison with the exact solution revealed that this methodology is only valid when all fibers are in tension and when the fiber orientation span is small [125, 126]. Recently, another drawback of the structural tensor was revealed. It turns out that except for the case of uniform or close to uniform orientation dispersion, the distributions recovered from the structure tensor fit poorly to the data. This

stems from the fact that the second rank generalized structure tensor is associated with just the lowest ranked term in a Fourier series expansion of the orientation distribution based on spherical functions, and it contains the least amount of information on the distribution compared to higher order terms in the expansion [51].

A second class of methodologies used to reduce the structural representation, attempts to simulate the tissue properties by a discrete set of fiber-bundles. One method was developed for amorphous polymers, and represents the tissue properties by an eight-chain, three-dimensional rectangle unit cell, whose shape determines the tissue orthotropy [127]. While this unit cell is a structure, it is unrelated to the real tissue structure. The two other methods represent the tissue's continuous 3D orientation distribution by a discrete set of fibers. In the first, the fibers in the set have fixed orientations, and weight is assigned to each set to optimize the fit to the tissue response [128]. This approach was shown, however, to introduce undesirable anisotropy to an isotropic material [129, 130]. The second variant applies the spherical t-design [131, 132], which is a set of N points on a sphere (or their equivalent fiber orientation), such that the average value of any polynomial f of degree t or less on this set equals the integral of f over the sphere. Hence, integration over the 3D orientation distribution is replaced by a sum of discrete values of that function. The design degree t depends on the orientation distribution function and on the fiber material law [133]. Hence, the polynomial degree t must be evaluated for each case [134] and may change as parameter estimates evolve during iterative search for optimal parameters during the process of tissue material characterization.

To summarize, at present, there seem to be no reliable reduced representation of tissue structure which could serve as an alternative to the orientation distribution function. This challenge is yet to be met.

Clinical Applications of the G&R Model: A number of pathologies are closely related to a remodeling transition from stable healthy state into an unstable diseased state. Two examples are cardiac hypertrophy (CH) and abdominal aortic aneurism (AAA). Untreated maladaptive CH leads to heart failure which is a leading cause of morbidity and has a 5-year mortality rate of 50 %. CH is a response to stress overload or to a disease. There are two types of CH. Eccentric hypertrophy is associated with increased chamber volume without change in the wall thickness, and can result from myocardial infarct (MI) damage to the myocardium or from mitral valve regurgitation. Structurally, increased chamber volume results from remodeling of the collagen network of the heart (which is predominant in its passive diastolic function), and an associated increase in the number and length of sarcomeres in series, thus leading to myocytes lengthening. The second type is concentric hypertrophy, which is associated with increased wall thickness and may arise from increased systolic ventricle pressure under hypertension or from aortic valve stenosis. Structurally, the wall thickens due to over-stress-induced increased in the number of parallel sarcomeres in the myocytes. Clinically, it is well known that mild to moderate left ventricle hypertrophy such as observed in training athletes, need not be pathological and may actually enhance cardiac performance (adaptive hypertrophy). The challenges are to identify the mechanical and biological culprits which lead to a pathological transition, and to establish the clinical threshold of transition from adaptive to maladaptive hypertrophy. Multi-scale structural characterization provides a predictive modeling platform for myocardial G&R that is realistically based on the physical tissue constituents and incorporates their measured mechano-biology into predictable and measurable function, thereby facilitating reliable clinical decisions.

AAA is an enlargement of the aorta, which result from deterioration of the elastin network in the vessel wall. The elastin function in resisting the dynamic luminal blood pressure

can be compensated by increased production of the other wall constituents (SMCs and collagen). The important clinical goal is to establish the thresholds of transition from a stable into an unstable state, which may lead to dissection and life-threatening massive internal bleeding. Here again, multi-scale modeling provides a straightforward platform for incorporation of measurable mechano-biological features of tissue constituents and their integration into global clinical measures.

Cellular Mechano-Biology: Cells are constantly exposed to mechanical forces in the body. In fact cells require a homeostatic mechanical environment in order to survive and proliferate [29]. Forces affect and control cell shape and biological functions, including gene expression, metabolism, secretion of biological factors, apoptosis (programed cell death), and modification of their ECM structure and properties, via turnover of fibers. Cells are exquisite sensors of their mechanical environment. Depending on the species, tissue and cell type, cells are sensitive to the nature of applied forces (tension/compression, pressure, shear), and to their magnitude, waveform and duration. For example, proteoglycan synthesis in chondrocytes (cells of the articular cartage) was found to be suppressed by static compression of up to 50 % strain, but cyclic compression has varied effects, depending on the loading regimen [135–138]: dynamic loading of 15 % at 0.3 Hz of chondrocytes seeded in agarose, decreased GAG synthesis, while under 1 Hz frequency increased it [139]. Many functions of endothelial cells (cells lining the blood vessel inner surface) are regulated by the blood shear stress [140]. Cyclic stretch was found to enhance the proliferation of human myocytes seeded in a gelatin matrix [141], and to increase elastin production by SMCs seeded in polymeric scaffold [142].

Cells mechano-biology is of fundamental importance in tissue engineering (TE) which aims to replace diseased native tissues with *in vitro* generated functional biological constructs that possess suitable structure and mechanical properties. Yet, a major obstacle to production of engineered tissues is the limited understanding of the mechanics-biology interrelationships between forces and cells' functions. The specific forces and regimes (magnitude, frequency, duration and waveform) which induce specific biological response are insufficiently understood. Comprehensive understanding can be achieved through well controlled experiments and realistic computational analysis of the mechanical forces experienced by the cells.

Design and Fabrication of Engineered Tissue: The goal of tissue engineering is to develop biological substitutes that restore, maintain, or improve function of native tissues, or of a whole organ [143]. Generation of an engineered tissue featuring specific structure and mechanical properties is an endeavor complementary to cell mechano-biology research. Knowledge gained from the research can be integrated into G&R-related modeling and design of the requisite materials and bioreactor protocols, which should lead to evolution of *in vitro* manufactured constructs to target engineered tissues. While the concepts and frameworks of this emerging sub-discipline are just beginning to be formulated, it is reasonable to expect that the multi-scale G&R structural theory presented above, will play a central role due to its versatility and realism in simulating the structure and biological remodeling that occur in the tissue substitute. With this achieved, the art of tissue engineering will be established on principles parallel to those of classical engineering design.

6.5 Concluding Comments

The research field of tissue mechanics is in its formative period. It is characterized by revolutionary transformation from the realm of classical continuum mechanics, typical of the

early years of the field just four decades ago, towards its own new identity. New concepts and tools are being developed to cope with the special challenges presented by the complex behavioral features of tissues, concepts which were hitherto unknown in classical mechanics. The present period is reminiscent of the formative developments in 1950s for the Theory of Plasticity, in the 1960s for Fracture Mechanics, and in the 1970–80s for Composite Materials. The field is experiencing an ongoing merge of biology, anatomy, physiology, bio-chemistry and physical chemistry into concepts and tools of non-linear continuum and structural mechanics. This results not only in improved realism of tissue characterization, but also in expansion of scope and creation of new fronts for classical mechanics towards more general response features such as activation, remodeling, and changing body mass.

Research in tissue mechanics is both important and rewarding. It holds the promise for most significant potential contributions to community health, by deciphering underlying mechanisms of physio-pathological processes, thereby paving the way towards development of protective and therapeutic measures, anti-aging strategies, and tissue engineered substitutes. The research work itself is highly rewarding, offering new, challenging and rich experience, due to its inter- and multi-disciplinary nature. It incorporates and integrates non-linear mechanics, mathematics, physiology, biology and chemistry. It is not surprising to find that as a result of these new horizons, interesting challenges in mechanics and material characterization present themselves. The topics presented here are just a few examples.

References

1. Fung, Y.C.: Elasticity of soft tissues in simple elongation. Physiol. Entomol. **213**(6), 1532–1544 (1967)
2. Lanir, Y.: Autobiographical postscript. In: Kassab, G.S., Sacks, M.S. (eds.) Structure-Based Mechanics of Tissues and Organs. Springer, New York (2016). pp. v–xxi
3. Humphrey, J.D.: From stress-strain relations to growth and remodeling theories: a historical reflection on microstructurally motivated constitutive relations. In: Kassab, G.S., Sacks, M.S. (eds.) Structure-Based Mechanics of Tissues and Organs, pp. 123–133. Springer, New York (2016)
4. Fratzl, P. (ed.) Collagen Structure and Mechanics, p. 508. Springer, New York (2008)
5. Ross, R., Fialkov, P.J., Altman, L.K.: The Moorphogenesis of Elasic Fibers. In: Sandberg, L.B., Gray, W.R., Franzblau, C. (eds.) Elastin and Elastic Tissue, pp. 7–17. Plenum Press, New York (1977)
6. Borg, T.K., Caulfield, J.B.: Collagen in the heart. Tex. Rep. Biol. Med. **39**, 321–333 (1979)
7. Borg, T.K., Caulfield, J.B.: Association of collagen struts with cardiac myocytes. J. Cell Biol. **87**(2), A126–A126 (1980)
8. Maroudas, A.: Balance between swelling pressure and collagen tension in normal and degenerate cartilage. Nature **260**(5554), 808–809 (1976)
9. Eckert, C.E., Fan, R., Mikulis, B., Barron, M., Carruthers, C.A., Friebe, V.M., Vyavahare, N.R., Sacks, M.S.: On the biomechanical role of glycosaminoglycans in the aortic heart valve leaflet. Acta Biomater. **9**(1), 4653–4660 (2013)
10. Emery, J.L., Omens, J.H., McCulloch, A.D.: Strain softening in rat left ventricular myocardium. J. Biomech. Eng. **119**(1), 6–12 (1997)
11. Fung, Y.C.: Stree-strain-history relations of soft tissues in simple elongation. In: Fung, Y.C., Perrone, N., Anliker, M. (eds.) Biomechanic—Its Foundations and Objectives, pp. 181–208. Prentice-Hall, Englewood Cliffs (1972)
12. Gregersen, H., Emery, J.L., McCulloch, A.D.: History-dependent mechanical behavior of Guinea-pig small intestine. Ann. Biomed. Eng. **26**(5), 850–858 (1998)
13. Lanir, Y., Fung, Y.C.: 2-dimensional mechanical-properties of rabbit skin. 2. Experimental results. J. Biomech. **7**(2), 171 (1974)
14. Lokshin, O., Lanir, Y.: Micro and macro rheology of planar tissues. Biomaterials **30**(17), 3118–3127 (2009)
15. Sverdlik, A., Lanir, Y.: Time-dependent mechanical behavior of sheep digital tendons, including the effects of preconditioning. J. Biomech. Eng. **124**(1), 78–84 (2002)

16. Chuong, C.J., Fung, Y.C.: On residual stresses in arteries. J. Biomech. Eng. **108**(2), 189–192 (1986)
17. Vaishnav, R.N., Vossoughi, J.: Estimation of residual strains in aortic segments. In: Hall, C.W. (ed.) Biomedical Engineering II: Recent Developments, pp. 330–333. Pergamon, New York (1983)
18. Lanir, Y., Hayam, G., Abovsky, M., Zlotnick, A.Y., Uretzky, G., Nevo, E., BenHaim, S.A.: Effect of myocardial swelling on residual strain in the left ventricle of the rat. Am. J. Physiol., Heart Circ. Physiol. **270**(5), H1736–H1743 (1996)
19. Omens, J.H., Fung, Y.C.: Residual strain in rat left ventricle. Circ. Res. **66**(1), 37–45 (1990)
20. Lanir, Y.: Mechanisms of residual stress in soft tissues. J. Biomech. Eng. **131**(4) (2009)
21. Lanir, Y.: Osmotic swelling and residual stress in cardiovascular tissues. J. Biomech. **45**(5), 780–789 (2012)
22. Fung, Y.C.: What are the residual stresses doing in our blood vessels? Ann. Biomed. Eng. **19**(3), 237–249 (1991)
23. Fung, Y.C., Liu, S.Q.: Strain distribution in small blood vessels with zero-stress state taken into consideration. Physiol. Entomol. **262** (2 Pt 2), H544–H552 (1992)
24. Brown, I.A.: A scanning electron microscope study of the effects of uniaxial tension on human skin. Br. J. Dermatol. **89**(4), 383–393 (1973)
25. Chu, B.M., Frasher, W.G., Wayland, H.: Hysteretic behavior of soft living animal tissue. Ann. Biomed. Eng. **1**(2), 182–203 (1972)
26. Viidik, A., Ekholm, R.: Light and electron microscopic studies of collagen fibers under strain. Z. Anat. Entwickl. Gesch. **127**, 154–164 (1968)
27. Butler, D.L., Grood, E.S., Noyes, F.R., Zernicke, R.F., Brackett, K.: Effects of structure and strain measurement technique on the material properties of young human tendons and fascia. J. Biomech. **17**(8), 579–596 (1984)
28. Aaron, B.B., Gosline, J.M.: Elastin as a random-network elastomer—a mechanical and optical analysis of single elastin fibers. Biopolymers **20**(6), 1247–1260 (1981)
29. Grinnell, F.: Fibroblasts, myofibroblasts, and wound contraction. J. Cell Biol. **124**(4), 401–404 (1994)
30. Eastwood, M., Porter, R., Khan, U., McGrouther, G., Brown, R.: Quantitative analysis of collagen gel contractile forces generated by dermal fibroblasts and the relationship to cell morphology. J. Cell. Physiol. **166**(1), 33–42 (1996)
31. Harris, A.K., Stopak, D., Wild, P.: Fibroblast traction as a mechanism for collagen morphogenesis. Nature **290**(5803), 249–251 (1981)
32. Pourati, J., Maniotis, A., Spiegel, D., Schaffer, J.L., Butler, J.P., Fredberg, J.J., Ingber, D.E., Stamenovic, D., Wang, N.: Is cytoskeletal tension a major determinant of cell deformability in adherent endothelial cells? Physiol. Entomol. **274**(5 Pt 1), C1283–C1289 (1998)
33. Kumar, S., Maxwell, I.Z., Heisterkamp, A., Polte, T.R., Lele, T.P., Salanga, M., Mazur, E., Ingber, D.E.: Viscoelastic retraction of single living stress fibers and its impact on cell shape, cytoskeletal organization, and extracellular matrix mechanics. Biophys. J. **90**(10), 3762–3773 (2006)
34. Fung, Y.C.: Biomechanics: Mechanical Properties of Living Tissues, 2nd edn. Springer, New York (1993). xviii, 568 p.
35. Murphy, R.A.: Mechanics of smooth muscle. In: Bohr, D.F., Somlyo, A.P., Sparks, A.V.J. (eds.) Handbook of Physiology, Sect. 2: The Cardiovascular System, pp. 325–351. American Physiological Society Bathesda (1980)
36. Bosse, Y., Solomon, D., Chin, L.Y., Lian, K., Pare, P.D., Seow, C.Y.: Increase in passive stiffness at reduced airway smooth muscle length: potential impact on airway responsiveness. Am. J. Physiol., Lung Cell. Mol. Physiol. **298**(3), L277–L287 (2010)
37. Herrera, A.M., McParland, B.E., Bienkowska, A., Tait, R., Pare, P.D., Seow, C.Y.: 'Sarcomeres' of smooth muscle: functional characteristics and ultrastructural evidence. J. Cell Sci. **118**(Pt 113), 2381–2392 (2005)
38. Seow, C.Y., Pratusevich, V.R., Ford, L.E.: Series-to-parallel transition in the filament lattice of airway smooth muscle. J. Appl. Physiol. **89**(3), 869–876 (1985). 2000
39. Speich, J.E., Almasri, A.M., Bhatia, H., Klausner, A.P., Ratz, P.H.: Adaptation of the length-active tension relationship in rabbit detrusor. Am. J. Physiol., Ren. Fluid Electrolyte Physiol. **297**(4), F1119–F1128 (2009)
40. Wang, L., Pare, P.D., Seow, C.Y.: Selected contribution: effect of chronic passive length change on airway smooth muscle length-tension relationship. J. Appl. Physiol. **90**(2), 734–740 (1985). 2001
41. Sacks, M.D.: In: Kassab, G.S., Sacks, M.S. (eds.) Finite Element Implementation of Structural Constitutive Models in Structure-Based Mechanics of Tissues and Organs, pp. 347–363. Springer, New York (2016)
42. Nguyen, T.D.: Biomechanics of the cornea and sclera. In: Kassab, G.S., Sacks, M.S. (eds.) Structure-Based Mechanics of Tissues and Organs, pp. 285–315. Springer, New York (2016)

43. Lee, L.C., Wenk, J., Klepach, D., Kassab, G.S., Guccione, J.M.: Structure-based models of ventricular myocardium. In: Kassab, G.S., Sacks, M.S. (eds.) Structure-Based Mechanics of Tissues and Organs, pp. 249–263. Springer, New York (2016)

44. Krishnamurthy, A., Coppola, B., Tangney, J., Kerckhoffs, R.C.P., McCulloch, A.D.: A microstructurally based multi-scale constitutive model of active myocardial mechanics. In: Kassab, G.S., Sacks, M.S. (eds.) Structure-Based Mechanics of Tissues and Organs, pp. 439–460. Springer, New York (2016)

45. Jor, J.W.Y., Babarenda Gamage, T.P., Nielsen, P.M.F., Nash, M.P., Hunter, P.J.: Relationship between structure and mechanics for membranous tissues. In: Kassab, G.S., Sacks, M.S. (eds.) Structure-Based Mechanics of Tissues and Organs, pp. 135–173. Springer, New York (2016)

46. Grytz, R., Meschke, G., Jonas, J.B., Downs, C.: Glaucoma and structure-based mechanics of the lamina cribrosa at multiple scales. In: Kassab, G.S., Sacks, M.S. (eds.) Structure-Based Mechanics of Tissues and Organs, pp. 93–122. Springer, New York (2016)

47. Gasser, T.C.: Histomechanical modeling of the wall of abdominal aortic aneurysm. In: Kassab, G.S., Sacks, M.S. (eds.) Structure-Based Mechanics of Tissues and Organs, pp. 57–78. Springer, New York (2016)

48. Cortes, D.H., Elliott, D.M.: Modeling of collageneous tissues using distributed fiber orientation. In: Kassab, G.S., Sacks, M.S. (eds.) Structure-Based Mechanics of Tissues and Organs, pp. 15–39. Springer, New York (2016)

49. Chen, H., Zhao, X., Lu, X., Kassab, G.S.: Microstructure-based constitutive models for coronary artery adventitia. In: Kassab, G.S., Sacks, M.S. (eds.) Structure-Based Mechanics of Tissues and Organs, pp. 225–248. Springer, New York (2016)

50. Bilston, L.E.: The influence of microstructure on neural tissue mechanics. In: Kassab, G.S., Sacks, M.S. (eds.) Structure-Based Mechanics of Tissues and Organs, pp. 1–14. Springer, New York (2016)

51. Lanir, Y., Namani, R.: Reliability of structure tensors in representing soft tissues structure. J. Mech. Behav. Biomed. Mater. **46**, 222–228 (2015)

52. Fan, R., Sacks, M.S.: Simulation of planar soft tissues using a structural constitutive model: finite element implementation and validation. J. Biomech. **47**(9), 2043–2054 (2014)

53. Rezakhaniha, R., Agianniotis, A., Schrauwen, J.T., Griffa, A., Sage, D., Bouten, C.V., van de Vosse, F.N., Unser, M., Stergiopulos, N.: Experimental investigation of collagen waviness and orientation in the arterial adventitia using confocal laser scanning microscopy. Biomech. Model. Mechanobiol. **11**(3–4), 461–473 (2012)

54. Viidik, A.: Simultaneous mechanical and light microscopic studies of collagen fibers. Z. Anat. Entwicklungsgesch. **136**(2), 204–212 (1972)

55. Evans, J.H., Barbenel, J.C., Steel, T.R., Ashby, A.M.: Structure and mechanics of tendon. Symp. Soc. Exp. Biol. **34**, 465–469 (1980)

56. Lanir, Y.: A structural theory for the homogeneous biaxial stress-strain relationships in flat collagenous tissues. J. Biomech. **12**(6), 423–436 (1979)

57. Lanir, Y.: Constitutive equations for fibrous connective tissues. J. Biomech. **16**(1), 1–12 (1983)

58. Lee, C.H., Zhang, W., Liao, J., Carruthers, C.A., Sacks, J.I., Sacks, M.S.: On the presence of affine fibril and fiber kinematics in the mitral valve anterior leaflet. Biophys. J. **108**(8), 2074–2087 (2015)

59. Holzapfel, G.A., Gasser, T.C., Ogden, R.W.: A new constitutive framework for arterial wall mechanics and a comparative study of material models. J. Elasticity **61**(1–3), 1–48 (2000)

60. Humphrey, J.D.: An evaluation of pseudoelastic descriptors used in arterial mechanics. J. Biomech. Eng. **121**(2), 259–262 (1999)

61. Lanir, Y.: Plausibility of structural constitutive equations for swelling tissues—implications of the C-N and S-E conditions. J. Biomech. Eng. **118**(1), 10–16 (1996)

62. Hollander, Y., Durban, D., Lu, X.A., Kassab, G.S., Lanir, Y.: Experimentally validated microstructural 3D constitutive model of coronary arterial media. J. Biomech. Eng. **133**(3) (2011)

63. Lu, X., Yang, J., Zhao, J.B., Gregersen, H., Kassab, G.S.: Shear modulus of porcine coronary artery: contributions of media and adventitia. Am. J. Physiol., Heart Circ. Physiol. **285**(5), H1966–H1975 (2003)

64. Wang, C., Garcia, M., Lu, X., Lanir, Y., Kassab, G.S.: Three-dimensional mechanical properties of porcine coronary arteries: a validated two-layer model. Am. J. Physiol., Heart Circ. Physiol. **291**(3), H1200–H1209 (2006)

65. Hollander, Y., Durban, D., Lu, X., Kassab, G.S., Lanir, Y.: Constitutive modeling of coronary arterial media-comparison of three model classes. J. Biomech. Eng. **133**(6) (2011)

66. Katchalsky, A.C., Peter, F.: Nonequilibrium Thermodynamics in Biophysics. Cambridge University Press, Cambridge (1967)

67. Richards, E.G.: An Introduction to the Physical Properties of Large Molecules in Solution. Cambridge University Press, Cambridge, U.K. (1980)

68. Truesdell, C.: Mechanical basis of diffusion. J. Chem. Phys. **37**, 2336–2344 (1962)
69. Lanir, Y.: Biorheology and fluid flux in swelling tissues. 1. Bicomponent theory for small deformations, including concentration effects. Biorheology **24**(2), 173–187 (1987)
70. Rodriguez, E.K., Hoger, A., McCulloch, A.D.: Stress-dependent finite growth in soft elastic tissues. J. Biomech. **27**(4), 455–467 (1994)
71. Skalak, R., Zargaryan, S., Jain, R.K., Netti, P.A., Hoger, A.: Compatibility and the genesis of residual stress by volumetric growth. J. Math. Biol. **34**(8), 889–914 (1996)
72. Taber, L.A., Humphrey, J.D.: Stress-modulated growth, residual stress, and vascular heterogeneity. J. Biomech. Eng. **123**(6), 528–535 (2001)
73. Azeloglu, E.U., Albro, M.B., Thimmappa, V.A., Ateshian, G.A., Costa, K.D.: Heterogeneous transmural proteoglycan distribution provides a mechanism for regulating residual stresses in the aorta. Am. J. Physiol., Heart Circ. Physiol. **294**(3), H1197–H1205 (2008)
74. Greenwald, S.E., Moore, J.E. Jr., Rachev, A., Kane, T.P., Meister, J.J.: Experimental investigation of the distribution of residual strains in the artery wall. J. Biomech. Eng. **119**(4), 438–444 (1997)
75. Stergiopulos, N., Vulliemoz, S., Rachev, A., Meister, J.J., Greenwald, S.E.: Assessing the homogeneity of the elastic properties and composition of the pig aortic media. J. Vasc. Res. **38**(3), 237–246 (2001)
76. Guo, X.M., Lanir, Y., Kassab, G.S.: Effect of osmolarity on the zero-stress state and mechanical properties of aorta. Am. J. Physiol., Heart Circ. Physiol. **293**(4), H2328–H2334 (2007)
77. Thornton, G.M., Oliynyk, A., Frank, C.B., Shrive, N.G.: Ligament creep cannot be predicted from stress relaxation at low stress: a biomechanical study of the rabbit medial collateral ligament. J. Orthop. Res. **15**(5), 652–656 (1997)
78. Raz, E., Lanir, Y.: Recruitment viscoelasticity of the tendon. J. Biomech. Eng. **131**(11), 111008 (2009)
79. Eshel, H., Lanir, Y.: Effects of strain level and proteoglycan depletion on preconditioning and viscoelastic responses of rat dorsal skin. Ann. Biomed. Eng. **29**(2), 164–172 (2001)
80. Mullins, L.: Softening of rubber by deformation. Rubber Chem. Technol. **42**, 339–362 (1969)
81. Tong, P., Fung, Y.C.: The stress-strain relationship for the skin. J. Biomech. **9**(10), 649–657 (1976)
82. Chuong, C.J., Fung, Y.C.: Compressibility and constitutive equation of arterial wall in radial compression experiments. J. Biomech. **17**(1), 35–40 (1984)
83. Fung, Y.C., Fronek, K., Patitucci, P.: Pseudoelasticity of arteries and the choice of its mathematical expression. Physiol. Entomol. **237**(5), H620–H631 (1979)
84. Lanir, Y.: Biaxial stress-strain relationship in the skin. Isr. J. Technol. **17**(2), 78–85 (1979)
85. Vawter, D.L., Fung, Y.C., West, J.B.: Constitutive equation of lung-tissue elasticity. J. Biomech. Eng. **101**(1), 38–45 (1979)
86. Humphrey, J.D., Vawter, D.L., Vito, R.P.: Pseudoelasticity of excised visceral pleura. J. Biomech. Eng. **109**(2), 115–120 (1987)
87. Yin, F.C.: Ventricular wall stress. Circ. Res. **49**(4), 829–842 (1981)
88. Glass, L., Hunter, P.J., McCulloch, A.D. (eds.): Theory of Heart. Springer, New York (1991)
89. Schnid, H., Hunter, P.J.: Multi-scale modeling of the heart. In: Holzapfel, G.A., Ogden, R.W. (eds.) Biomechanical Modeling at the Molecular, Cellular and Tissue Levels, pp. 83–107. Springer, Wien (2009)
90. Frank, J.S., Langer, G.A.: The myocardial interstitium: its structure and its role in ionic exchange. J. Cell Biol. **60**(3), 586–601 (1974)
91. Caspari, P.G., Newcomb, M., Gibson, K., Harris, P.: Collagen in the normal and hypertrophied human ventricle. Cardiovasc. Res. **11**(6), 554–558 (1977)
92. Weber, K.T.: Cardiac interstitium in health and disease: the fibrillar collagen network. J. Am. Coll. Cardiol. **13**(7), 1637–1652 (1989)
93. Streeter, D.D. Jr., Spotnitz, H.M., Patel, D.P., Ross, J. Jr., Sonnenblick, E.H.: Fiber orientation in the canine left ventricle during diastole and systole. Circ. Res. **24**(3), 339–347 (1969)
94. Borg, T.K., Caulfield, J.B.: The collagen matrix of the heart. Fed. Proc. **40**(7), 2037–2041 (1981)
95. Caulfield, J.B., Borg, T.K.: The collagen network of the heart. Labor Invest. **40**(3), 364–372 (1979)
96. Robinson, T.F., Cohen-Gould, L., Factor, S.M.: Skeletal framework of mammalian heart muscle: arrangement of inter- and pericellular connective tissue structures. Labor Invest. **49**(4), 482–498 (1983)
97. Robinson, T.F., Factor, S.M., Capasso, J.M., Wittenberg, B.A., Blumenfeld, O.O., Seifter, S.: Morphology, composition, and function of struts between cardiac myocytes of rat and hamster. Cell Tissue Res. **249**(2), 247–255 (1987)
98. Caulfield, J.B., Borg, T.K.: Collagen network of the heart. Lab. Invest. **40**(3), 364–372 (1979)
99. Horowitz, A., Lanir, Y., Yin, F.C.P., Perl, M., Sheinman, I., Strumpf, R.K.: Structural 3-dimensional constitutive law for the passive myocardium. J. Biomech. Eng. **110**(3), 200–207 (1988)
100. Nevo, E., Lanir, Y.: Structural finite deformation model of the left-ventricle during diastole and systole. J. Biomech. Eng. **111**(4), 342–349 (1989)

101. Labeit, S., Kolmerer, B.: Titins: giant proteins in charge of muscle ultrastructure and elasticity. Science **270**(5234), 293–296 (1995)
102. Hill, A.V.: The heat of shortening and the dynamic constants of muscle. Proc. R. Soc. Edinb. Sect. B. Biol. **126**, 136–195 (1938)
103. Jockenhoevel, S., Zund, G., Hoerstrup, S.P., Schnell, A., Turina, M.: Cardiovascular tissue engineering: a new laminar flow chamber for in vitro improvement of mechanical tissue properties. ASAIO J. **48**(1), 8–11 (2002)
104. Nerem, R.M., Seliktar, D.: Vascular tissue engineering. Annu. Rev. Biomed. Eng. **3**, 225–243 (2001)
105. Niklason, L.E., Yeh, A.T., Calle, E.A., Bai, Y., Valentin, A., Humphrey, J.D.: Enabling tools for engineering collagenous tissues integrating bioreactors, intravital imaging, and biomechanical modeling. Proc. Natl. Acad. Sci. USA **107**(8), 3335–3339 (2010)
106. Jackson, Z.S., Gotlieb, A.I., Langille, B.L.: Wall tissue remodeling regulates longitudinal tension in arteries. Circ. Res. **90**(8), 918–925 (2002)
107. Kamiya, A., Togawa, T.: Adaptive regulation of wall shear stress to flow change in the canine carotid artery. Am. J. Physiol. **239**(1), H14–H21 (1980)
108. Langille, B.L., Bendeck, M.P., Keeley, F.W.: Adaptations of carotid arteries of young and mature rabbits to reduced carotid blood flow. Am. J. Physiol. **256**(4 Pt 2), H931–H939 (1989)
109. Wayman, B.H., Taylor, W.R., Rachev, A., Vito, R.P.: Arteries respond to independent control of circumferential and shear stress in organ culture. Ann. Biomed. Eng. **36**(5), 673–684 (2008)
110. Humphrey, J.D., Rajagopal, K.R.: A constrained mixture model for growth and remodeling of soft tissues. Math. Models Methods Appl. Sci. **12**(3), 407–430 (2002)
111. Cowin, S.C.: Tissue growth and remodeling. Annu. Rev. Biomed. Eng. **6**, 77–107 (2004)
112. Lanir, Y.: Mechanistic micro-structural theory of soft tissues growth and remodeling: tissues with unidirectional fibers. Biomech. Model. Mechanobiol. **14**(2), 245–266 (2015)
113. Gleason, R.L., Jr., Humphrey, J.D.: A 2D constrained mixture model for arterial adaptations to large changes in flow, pressure and axial stretch. Math. Med. Biol. **22**(4), 347–369 (2005)
114. Cowin, S.C.: Continuum kinematical modeling of mass increasing biological growth. Int. J. Eng. Sci. **48**(11), 1137–1145 (2010)
115. Chen, H., Liu, Y., Slipchenko, M.N., Zhao, X., Cheng, J.X., Kassab, G.S.: The layered structure of coronary adventitia under mechanical load. Biophys. J. **101**(11), 2555–2562 (2011)
116. Hill, M.R., Duan, X., Gibson, G.A., Watkins, S., Robertson, A.M.: A theoretical and non-destructive experimental approach for direct inclusion of measured collagen orientation and recruitment into mechanical models of the artery wall. J. Biomech. **45**(5), 762–771 (2012)
117. Horny, L., Chlup, H., Zitny, R.: Collagen orientation and waviness within the vein wall. In: XI International Conference on Computational Plasticity: Fundamentals and Applications, Spain. International Center for Numerical Methods in Engineering (CIMNE), Barcelona (2011)
118. Zeinali-Davarani, S., Chow, M.J., Turcotte, R., Zhang, Y.: Characterization of biaxial mechanical behavior of porcine aorta under gradual elastin degradation. Ann. Biomed. Eng. **41**(7), 1528–1538 (2013)
119. Chen, H., Liu, Y., Zhao, X.F., Lanir, Y., Kassab, G.S.: A micromechanics finite-strain constitutive model of fibrous tissue. J. Mech. Phys. Solids **59**(9), 1823–1837 (2011)
120. Imanuel, O.: Stress analysis in the left ventricle of the heart. PhD thesis, Faculty of Biomedical Engineering, Technion–I.I.T.: Haifa (1996)
121. Chen, H., Liu, Y., Slipchenko, M., Zhao, X., Cheng, J.-X., Kassab, G.: The layered structure of coronary adventitia under mechanical load. Biophys. J. **101**, 2555–2562 (2011). doi:10.1016/j.bpj.2011.10.043
122. Zoumi, A., Lu, X., Kassab, G.S., Tromberg, B.J.: Imaging coronary artery microstructure using second-harmonic and two-photon fluorescence microscopy. Biophys. J. **87**(4), 2778–2786 (2004)
123. Freed, A.D., Einstein, D.R., Vesely, I.: Invariant formulation for dispersed transverse isotropy in aortic heart valves: an efficient means for modeling fiber splay. Biomech. Model. Mechanobiol. **4**(2–3), 100–117 (2005)
124. Gasser, T.C., Ogden, R.W., Holzapfel, G.A.: Hyperelastic modelling of arterial layers with distributed collagen fibre orientations. J. Roy. Soc. Interface **3**, 15–35 (2006)
125. Cortes, D.H., Lake, S.P., Kadlowec, J.A., Soslowsky, L.J., Elliott, D.M.: Characterizing the mechanical contribution of fiber angular distribution in connective tissue: comparison of two modeling approaches. Biomech. Model. Mechanobiol. **9**(5), 651–658 (2010)
126. Federico, S., Herzog, W.: Towards an analytical model of soft biological tissues. J. Biomech. **41**(16), 3309–3313 (2008)
127. Bischoff, J.E., Arruda, E.A., Grosh, K.: A microstructurally based orthotropic hyperelastic constitutive law. J. Appl. Mech. **69**, 570–579 (2002)
128. Elata, D., Rubin, M.: Isotropy of strain energy functions which depend only on a finite number of directional strain measures. J. Appl. Mech. **61**(2), 284–289 (1994)

129. Bazant, Z.P.: Efficient numerical integration on the surface of a sphere. ZAMM Z. Angew. Math. Mech. **66**(1), 37–49 (1986)

130. Ehret, A.E., Itskov, M., Schmid, H.: Numerical integration on the sphere and its effect on the material symmetry of constitutive equations—a comparative study. Internat. J. Numer. Methods Engrg. **81**(2), 189–206 (2010)

131. Delsarte, P., Goethals, J.M., Seidel, J.J.: Spherical codes and designs. Geom. Dedicata **6**, 363–388 (1977)

132. Hardin, R.H., Sloane, N.J.A.: McLaren's improved snub cube and other new spherical designs in three dimensions. Discrete Comput. Geom. **15**, 429–441 (1996)

133. Federico, S., Gasser, T.C.: Nonlinear elasticity of biological tissues with statistical fiber orientation. J. Roy. Soc. Interface **7**(47), 955–966 (2010)

134. Martufi, G., Gasser, T.C.: A constitutive model for vascular tissue that integrates fibril, fiber and continuum levels with application to the isotropic and passive properties of the infrarenal aorta. J. Biomech. **44**(14), 2544–2550 (2011)

135. Gray, M.L., Pizzanelli, A.M., Grodzinsky, A.J., Lee, R.C.: Mechanical and physiochemical determinants of the chondrocyte biosynthetic response. J. Orthop. Res. **6**(6), 777–792 (1988)

136. Palmoski, M.J., Brandt, K.D.: Effects of static and cyclic compressive loading on articular cartilage plugs in vitro. Arthritis Rheum. **27**(6), 675–681 (1984)

137. Sah, R.L., Kim, Y.J., Doong, J.Y., Grodzinsky, A.J., Plaas, A.H., Sandy, J.D.: Biosynthetic response of cartilage explants to dynamic compression. J. Orthop. Res. **7**(5), 619–636 (1989)

138. Torzilli, P.A., Grigiene, R., Huang, C., Friedman, S.M., Doty, S.B., Boskey, A.L., Lust, G.: Characterization of cartilage metabolic response to static and dynamic stress using a mechanical explant test system. J. Biomech. **30**(1), 1–9 (1997)

139. Lee, D.A., Bader, D.L.: Compressive strains at physiological frequencies influence the metabolism of chondrocytes seeded in agarose. J. Orthop. Res. **15**(2), 181–188 (1997)

140. Davies, P.F.: Flow-mediated endothelial mechanotransduction. Physiol. Rev. **75**(3), 519–560 (1995)

141. Akhyari, P., Fedak, P.W., Weisel, R.D., Lee, T.Y., Verma, S., Mickle, D.A., Li, R.K.: Mechanical stretch regimen enhances the formation of bioengineered autologous cardiac muscle grafts. Circulation **106**(12 Suppl 1), I137–I142 (2002)

142. Kim, B.S., Nikolovski, J., Bonadio, J., Mooney, D.J.: Cyclic mechanical strain regulates the development of engineered smooth muscle tissue. Nat. Biotechnol. **17**(10), 979–983 (1999)

143. Langer, R., Vacanti, J.P.: Tissue engineering. Science **260**(5110), 920–926 (1993)

144. Fung, Y.C.: Biorheology of soft tissues. Biorheology **10**(2), 139–155 (1973)